KfK 4791
September 1990

Stress Intensity Factors and Weight Functions for the Edge Cracked Plate Calculated by the Boundary Collocation Method

T. Fett
Institut für Material- und Festkörperforschung

Kernforschungszentrum Karlsruhe

KERNFORSCHUNGSZENTRUM KARLSRUHE
Institut für Material- und Festkörperforschung

KfK 4791

Stress intensity factors and weight functions for the edge cracked plate calculated by the boundary collocation method

T. Fett

Kernforschungszentrum Karlsruhe GmbH, Karlsruhe

Als Manuskript gedruckt

Kernforschungszentrum Karlsruhe GmbH
Postfach 3640, 7500 Karlsruhe 1

ISSN 0303-4003

Stress intensity factors and weight functions for the edge cracked plate calculated by the boundary collocation method

Abstract

The determination of stress intensity factors for cracks exposed to arbitrary stress distribution according to the weight function method calls for knowledge of the crack opening displacements and stress intensity factor for a reference load case. The determination of these variables by means of the **Boundary Collocation Method (BCM)** is discussed by the example of the drawn plate with an edge crack. After derivation of the formulas for evaluation the influence is studied of the relative crack depth and the plate length on the stress intensity factor, and the results are compared with data from the literature.
The crack opening displacement field is determined from the stress function established by the Boundary Collocation Method and the fracture mechanical weight function is calculated from it. The results are compared with an analytical weight function obtained on the basis of approximative crack opening displacement fields. A formula is indicated for the weight function which covers the total range from a/W = 0 to a/W = 1. This formula is the result of BCM computations made up to a/W = 0.8 for a relative plate length of a/H>1.5 and applies to the limit case a/W = 1 known from the analysis.
Finally the Boundary Collocation Method is used to calculate the mode II stress intensity factors for shear loaded plates with an edge crack. The results of the computations are compared with solutions proposed in the literature. For the edge crack loaded with constant shear stresses, which act on the crack surfaces, a numerical formula is given of the geometric function. Values applicable to the weight function are determined from the crack opening displacements.
As an example of application the weight functions h_I *and* h_{II} are used to calculate the stress intensity factors of edge-notched beams in an asymmetric bending-arrangement.

Spannungsintensitätsfaktoren und Gewichtsfunktionen für die Platte mit Außenriß auf der Basis der Boundary-Collocation-Methode

Kurzfassung

Die Ermittlung von Spannungsintensitätsfaktoren für Risse unter beliebiger Spannungsverteilung nach der Methode der Gewichtsfunktion erfordert die Kenntnis der Rißuferverschiebungen und des Spannungsintensitätsfaktors für einen Referenzlastfall. Die Bestimmung dieser Größen mittels der **Boundary-Collocation-Methode** wird am Beispiel der gezogenen Platte mit 'edge crack' behandelt. Nach Herleitung der Auswerteformeln werden der Einfluß der relativen Rißtiefe sowie der Plattenlänge auf den Spannungsintensitätsfaktor untersucht und die Ergebnisse mit Literaturdaten verglichen.
Aus der mit der Boundary-Collocation-Methode bestimmten Spannungsfunktion wird das Rißuferverschiebungsfeld ermittelt und daraus die bruchmechanische Gewichtsfunktion berechnet. Die Ergebnisse werden mit einer auf der Basis approximativer Rißuferverschiebungsfelder erhaltenen analytischen Gewichtsfunktion verglichen. Es wird eine Formel für die Gewichtsfunktion im gesamten Bereich von a/W = 0 bis a/W = 1 angegeben, die auf BCM-Rechnungen bis a/W = 0.8 bei einer relativen Plattenlänge von H/W>1.5 und auf dem analytisch bekannten Grenzfall a/W = 1 beruht.
Abschließend wird die "Boundary-Collocation"-Methode zur Berechnung der Mode-II-Spannungsintensitätsfaktoren für schubbelastete Platten mit Außenriß verwendet. Die Ergebnisse der Berechnungen werden mit Literaturlösungen verglichen. Im Falle des mit konstanten Schubspannungen auf den Rißflächen belasteten "edge-cracks" wird eine numerische Formel für die Geometriefunktion angegeben. Aus den Rißuferverschiebungen werden Werte der Gewichtsfunktion bestimmt.
In einem Anwendungsbeispiel - dem unsymmetrisch belasteten 4-Punkt-Biegestab mit Riß - werden die Spannungsintensitätsfaktoren K_I und K_{II} ermittelt.

Table of Contents

1. Introduction

The current determination of stress intensity factors by means of the weight function method calls for knowledge of the crack opening displacements (CODs) and stress intensity factor for a reference load case. Whereas approximation methods have been developed for the determination of the crack opening displacements, knowledge of the reference stress intensity factor is indispensable. One method of the analytical determination of K-factors is the **Boundary Collocation Method (BCM)** which was pioneered in early research activities by Gross, Srawley and Brown (e.g. [2] and [3]). Thanks to the conspicuous increase in the speed of computation of present-day computers this method continues to be highly important, not the least due to its high accuracy.
The computation of stress intensity factors can be reduced to the determination of the stress distribution at the crack tip, which is fully known if we succeed in the determination of the Airy stress function Φ.

2. Principles of the Boundary Collocation Method

2.1 *The Airy stress function for crack problems*

The stress components can be represented in polar coordinates - with the pole in the crack tip (fig.1) - as

$$\sigma_r = \frac{1}{r}\frac{\partial \Phi}{\partial r} + \frac{1}{r^2}\frac{\partial^2 \Phi}{\partial \varphi^2}$$

$$\sigma_\varphi = \frac{\partial^2 \Phi}{\partial r^2} \qquad (1)$$

$$\tau_{r\varphi} = \frac{1}{r^2}\frac{\partial \Phi}{\partial \varphi} - \frac{1}{r}\frac{\partial^2 \Phi}{\partial r \partial \varphi}$$

The orientation of these stresses is likewise indicated in fig.1. The Airy stress function results as a solution of the bipotential equation

$$\Delta\Delta\Phi = 0 \qquad (2)$$

In its extended version and represented in polar coordinates this gives

$$\left(\frac{\partial^2}{\partial r^2} + \frac{1}{r}\frac{\partial}{\partial r} + \frac{1}{r^2}\frac{\partial^2}{\partial \varphi^2}\right)\left(\frac{\partial^2 \Phi}{\partial r^2} + \frac{1}{r}\frac{\partial \Phi}{\partial r} + \frac{1}{r^2}\frac{\partial^2 \Phi}{\partial \varphi^2}\right) = 0 \qquad (3)$$

Besides the condition of compatibility (2), Φ and the stress components, respectively, have to fulfill in addition the boundary conditions still to be specified. Regarding the crack problem, the requirement must e.g. be fulfilled that the crack faces are free of stress, i.e.

$$\sigma_\varphi \,|_{\varphi=\pm\pi} = 0 \qquad (4a)$$

$$\tau_{r\varphi} \,|_{\varphi=\pm\pi} = 0 \qquad (4b)$$

Due to the linearity of eq.(2) the stress function Φ can be divided into a fraction Φ_s which is symmetric with respect to $\varphi = 0$ and an antisymmetric fraction Φ_a.

$$\Phi = \Phi_s + \Phi_a \qquad (5)$$

The general treatment of the crack problem will be explained here in more detail by the example of the symmetric fraction of the stress function.

2.2 *Approach to determine the stress function*

Expressions by a series are formulated for the still unknown stress function. For instance a power series could be developed to describe the dependence on the distance r and a Fourier series for the angular dependence. Their general term

$$\Phi_{s,\,\nu\mu} = A_{\nu\mu}\, r^\nu \cos \mu\varphi \qquad (6)$$

after introduction into (3) yields

$$\Delta\Delta\Phi_{s,\,\nu\mu} = A_{\nu\mu}\, r^{\nu-4}(\nu^2 - \mu^2)[(\nu-2)^2 - \mu^2]\cos(\mu\varphi) = 0 \qquad (7)$$

Since this relation must be fulfilled for any values of r and φ, the non-trivial solutions

$$\nu = \mu \quad \text{und} \quad \nu = \mu + 2 \qquad (8)$$

follow with

$$\Phi_\nu = r^\nu [A_{\nu 1} \cos \nu\varphi + A_{\nu 2} \cos(\nu - 2)\varphi] \tag{9}$$

Since no use has as yet been made of the integralness of ν, eq.(9) applies likewise to any value of ν, and the functions Φ_ν, consequently are eigenfunctions of the bipotential equation (2) with the eigenvalue ν. Therfore, a development by eigenfunctions is possible.
In this representation the stress function reads

$$\Phi_s = \sum_{\lambda \geq 3/2}^{\infty} r^\lambda [A_1 \cos \lambda\varphi + A_2 \cos(\lambda - 2)\varphi] \tag{10}$$

$$\Phi_a = \sum_{\lambda \geq 3/2}^{\infty} r^\lambda [B_1 \sin \lambda\varphi + B_2 \sin(\lambda - 2)\varphi] \tag{11}$$

with the summation to be made only over the eigenvalues $\lambda \geq 3/2$. Eigenvalues smaller than 3/2 do no longer give stresses capable of integration which means that the elastic energy diverges ahead of the crack tip!

2.3 *Consideration of the boundary conditions*

2.3.1 Free crack surfaces

Introduction of the expansions (10) und (11) into the conditions applicable to crack surfaces free of normal stress and shear stress according to eqs.(4a,4b) yields (in case of the symmetric portion) two relations

$$A_1 \cos \lambda\pi + A_2 \cos(\lambda - 2)\pi = 0 \tag{12a}$$

$$A_1 \lambda \sin \lambda\pi + A_2(\lambda - 2) \sin(\lambda - 2)\pi = 0 \tag{12b}$$

from which the eigenvalues λ and one coefficient each must be determined.
Equation (12a) is non-trivially fulfilled by

$$\cos \lambda\pi = \cos(\lambda - 2)\pi = 0 \quad \rightarrow \quad \lambda = \frac{3}{2}, \frac{5}{2} \ldots\ldots$$

and the solution of eq.(12b)

$$\sin \lambda_I^* \pi = \sin(\lambda_I^* - 2)\pi = 0 \quad \rightarrow \quad \lambda_I^* = 2,3,4 \ldots.$$

follows. The symbol $*$ is introduced here in order to discriminate between the two solutions
The coefficients pertaining to the two solutions are

$$A_2 = -A_1 \frac{\lambda}{\lambda - 2}$$

and

$$A_2^* = -A_1^*$$

2.3.2 Crack surfaces exposed to constant load

If the crack borders are loaded with the *constant pressure* $\mathbf{p_0}$, the symmetric stress function will include an additional term which, on account of the non-dependence of the pressure p_0 on the distance from the crack tip, can only take the form r^0. Then, instead of the boundary condition (12a) it follows

$$A_1 \cos \lambda\pi + A_2 \cos(\lambda - 2)\pi = 0 \quad \text{für} \quad \lambda > 2$$

and

$$A_1 \cos 2\pi + A_2 \cos 0 = \frac{p_0}{2} \quad \text{für} \quad \lambda = 2$$

Thus, the following additional term of the symmetric stress function is obtained

$$\delta\Phi_s = \frac{1}{2} p_0 r^2$$

If a crack is exposed to *constant shear stress* τ_0 on the crack faces a term is found in addition to the antisymmetric portion of the stress function

$$\delta\Phi_a = -\frac{1}{2} \tau_0 r^2 \sin 2\varphi$$

2.3.3 Stress function

The series (10) together with the eigenvalues and coefficients yield after appropriate renumbering of the running index

$$\Phi_s = \sum_{n=0}^{\infty} r^{n+3/2} A_n \left[\cos(n + 3/2)\varphi - \frac{n + 3/2}{n - 1/2} \cos(n - 1/2)\varphi \right]$$

$$+ \sum_{n=0}^{\infty} r^{n+2} A_n^* [\cos(n + 2)\varphi - \cos n\varphi] \qquad (13)$$

$$+ \frac{1}{2} p_0 r^2$$

where the first sum accounts for singular stress distribution and the second for the regular portion.a.ren Anteil verantwortlich.
In analogy, the following expression is obtained for the antisymmetric portion of the stress function

$$\Phi_a = \sum_{n=0}^{\infty} r^{n+3/2} B_n [\sin(n + 3/2)\varphi - \sin(n - 1/2)\varphi]$$

$$+ \sum_{n=0}^{\infty} r^{n+3} B_n^* \left[\sin(n + 3)\varphi - \frac{n + 3}{n + 1} \sin(n + 1)\varphi \right] \qquad (14)$$

$$- \frac{1}{2} \tau_0 r^2 \sin 2\varphi$$

2.4 Stresses

These are the stresses following from eq.(1):

symmetric portions

$$\sigma_r = \sum_{n=0}^{\infty} A_n r^{n-1/2}(n+3/2)\left[\frac{n^2-2n-5/4}{n-1/2}\cos(n-1/2)\varphi - (n+1/2)\cos(n+3/2)\varphi\right] \qquad (15a)$$

$$+ \sum_{n=0}^{\infty} A_n^* r^n\left[(n^2-n-2)\cos n\varphi - (n+2)(n+1)\cos(n+2)\varphi\right] + p_0$$

$$\sigma_\varphi = \sum_{n=0}^{\infty} A_n r^{n-1/2}(n+3/2)(n+1/2)\left[\cos(n+3/2)\varphi - \frac{n+3/2}{n-1/2}\cos(n-1/2)\varphi\right] \qquad (16a)$$

$$+ \sum_{n=0}^{\infty} A_n^* r^n(n+2)(n+1)[\cos(n+2)\varphi - \cos n\varphi] + p_0$$

$$\tau_{r\varphi} = \sum_{n=0}^{\infty} A_n r^{n-1/2}(n+3/2)(n+1/2)[\sin(n+3/2)\varphi - \sin(n-1/2)\varphi] \qquad (17a)$$

$$+ \sum_{n=0}^{\infty} A_n^* r^n(n+1)[(n+2)\sin(n+2)\varphi - n\sin n\varphi]$$

antisymmetric portions

$$\sigma_r = \sum_{n=0}^{\infty} B_n r^{n-1/2}\left[(n^2-2n-5/4)\sin(n-1/2)\varphi - (n+3/2)(n+1/2)\sin(n+3/2)\varphi\right] \qquad (15b)$$

$$+ \sum_{n=0}^{\infty} B_n^* r^{n+1}(n+3)\left[\frac{n^2+n-2}{n+1}\sin(n+1)\varphi - (n+2)\sin(n+3)\varphi\right]$$

$$+ \tau_0 \sin 2\varphi$$

$$\sigma_\varphi = \sum_{n=0}^{\infty} B_n r^{n-1/2}(n+3/2)(n+1/2)[\sin(n+3/2)\varphi - \sin(n-1/2)\varphi] \qquad (16b)$$

$$+ \sum_{n=0}^{\infty} B_n^* r^{n+1}(n+3)(n+2)\left[\sin(n+3)\varphi - \frac{n+3}{n+1}\sin(n+1)\varphi\right]$$

$$- \tau_0 \sin 2\varphi$$

$$\tau_{r\varphi} = \sum_{n=0}^{\infty} B_n r^{n-1/2}(n+1/2)[(n-1/2)\cos(n-1/2)\varphi - (n+3/2)\cos(n+3/2)\varphi] \qquad (17b)$$

$$- \sum_{n=0}^{\infty} B_n^* r^{n+1}(n+3)(n+2)[\cos(n+3)\varphi - \cos(n+1)\varphi]$$

$$+ \tau_0 \cos 2\varphi$$

In the special case of the **crack tip near-field** the terms proportional to $1/\sqrt{r}$ with $r \to 0$ are dominating. The associated stresses result from the **symmetric portion** of the stress function

$$\sigma_r = \frac{3}{4} A_0 r^{-1/2} [5 \cos \frac{1}{2}\varphi - \cos \frac{3}{2}\varphi] \tag{18a}$$

$$\sigma_\varphi = \frac{3}{4} A_0 r^{-1/2} [3 \cos \frac{1}{2}\varphi + \cos \frac{3}{2}\varphi] \tag{18b}$$

$$\tau_{r\varphi} = \frac{3}{4} A_0 r^{-1/2} [\sin \frac{1}{2}\varphi + \sin \frac{3}{2}\varphi] \tag{18c}$$

and from the **antisymmetric portion** of the stress function it follows

$$\sigma_r = -\frac{1}{4} B_0 r^{-1/2} [-5 \sin \frac{1}{2}\varphi + 3 \sin \frac{3}{2}\varphi] \tag{18d}$$

$$\sigma_\varphi = -\frac{1}{4} B_0 r^{-1/2} [-3 \sin \frac{1}{2}\varphi - 3 \sin \frac{3}{2}\varphi] \tag{18e}$$

$$\tau_{r\varphi} = -\frac{1}{4} B_0 r^{-1/2} [\cos \frac{1}{2}\varphi + 3 \cos \frac{3}{2}\varphi] \tag{18f}$$

These relations are identical with the Sneddon equations and thus allow A_0, A_0^* to be identified and likewise the stress intensity factors K_I, K_{II}, viz.,

$$K_I = 3\sqrt{2\pi}\, A_0 \tag{19a}$$

$$K_{II} = -\sqrt{2\pi}\, B_0 \tag{19b}$$

2.5 *Determination of the coefficients A,A**

For practical application of eqs.(13) and (14), which are used to determine stress intensity factors, the infinite series must be truncated after the Nth term for which an adequate value must be chosen.

The still unknown coefficients are determined by fitting of the stresses resulting from eqs.(15 to 17) to the specified boundary conditions. If for a selected number of 2(N+1) edge points two of the related stress components are known, two of eqs.(15) to (17) each yield a system of equations with 2(N+1) unknowns whose solutions allow all 2(N+1) coefficients of eqs.(13,14) to be determined. Frequently, the computation is reduced to only N+1 equations. This always holds when the problem is a purely symmetric one which will be described in the following section.

The expenditure in terms of computation can be reduced by selection of a rather large number of edge points and by solving subsequently the then overdetermined system of equations by use of the least squares of deviations, thus obtaining a set of "best" coefficients.

The Harwell subroutine V02AD is used here to determine the best fit. The nomber of fitting nodes was selected to be 4N.

The description of the boundary conditions by the given load stresses is meaningful, above all for stresses subjected to high local variations (e.g. bolt loading). elatively homogeneous loading (eg. constant tension, bending) fitting to the boundary conditions applicable to the stress function - which ss an integral variable is an average of the stresses - should be preferred. The determination of the boundary conditions of the stress function from the boundary conditions of stress is illustrated by the examples. der Spannung wird in den Beispielen verdeutlicht.

The fitting points should be selected such that their densities likewise increases with their approaching the the crack tip. One possibility is e.g. to choose equidistant angular steps between successive fitting points. Since the stress components in the rectangular coordinate system are known for the border - as in the case here - also the stress components given in eqs.(15-17) must be rewritten as

$$\sigma_x = \sigma_r \cos^2\varphi + \sigma_\varphi \sin^2\varphi - 2\tau_{r\varphi} \sin\varphi \cos\varphi \tag{20a}$$

$$\sigma_y = \sigma_r \sin^2\varphi + \sigma_\varphi \cos^2\varphi + 2\tau_{r\varphi} \sin\varphi \cos\varphi \tag{20b}$$

$$\tau_{xy} = (\sigma_r - \sigma_\varphi) \sin\varphi \cos\varphi + \tau_{r\varphi}(\cos^2\varphi - \sin^2\varphi) \tag{20c}$$

3. Edge cracked plate under mode I loading

3.1 *The plate subjected to tension*

The first practical example to be cited here ist the plate drawn in longitudinal direction, provided with a straight through crack on its side, length 2H, width W.
The stresses at the border in this example are

$$\sigma_x = 0 \quad , \quad \tau_{xy} = 0 \quad \text{für} \quad x = -a \tag{21a}$$

$$\sigma_y = \sigma_0 \quad , \quad \tau_{xy} = 0 \quad \text{für} \quad y = H \tag{21b}$$

$$\sigma_x = 0 \quad , \quad \tau_{xy} = 0 \quad \text{für} \quad x = W \tag{21c}$$

The stress σ_0 can be chosen arbitrarily because the only interesting result of computation is the geometric function which is determined by dividing again by σ_0. It is recommended to choose e.g. $\sigma_0 = 1$.
In the special case selected here of the drawn plate the study can be restricted to the symmetric stress components for reasons of symmetry (with respect to y=0). Due to the free crack surfaces one can set $p_0 = 0$.
The boundary conditions for the stresses given by eq.(21) can be rewritten by making reference to equivalent boundary conditions which are applicable to the stress function Φ_s.
Instead of ($r = a, \varphi = \pi$) the stress function according to eq.(13) is given by

$$\Phi_s|_{r,\,\pi} = \Phi_s|_{x=-a,y=0} = 0 \tag{21d}$$

Moreover, for partial derivations at the same location it applies am gleichen Ort

$$\partial\Phi_s/\partial x|_{x=-a,y=0} = 0 \tag{21e}$$

and

$$\partial\Phi_s/\partial y|_{x=-a,y=0} = 0 \tag{21f}$$

As both the shear stresses τ_{xy} and the normal stresses σ_x along the line x=-a disappear, the following expressions must hold for all locations y according to eq.(1):

$$\frac{\partial^2\Phi_s}{\partial x\partial y}|_{x=-a} = 0 \tag{21g}$$

$$\frac{\partial^2\Phi_s}{\partial y^2}|_{x=-a} = 0 \tag{21h}$$

Along the edge defined by y=H the shear stress disappears and the normal stress is $\sigma_y = \sigma_0 = 1$. It follows

$$\frac{\partial^2\Phi_s}{\partial x^2}|_{y=H} = \sigma_0 \tag{21i}$$

$$\frac{\partial^2\Phi_s}{\partial x\partial y}|_{y=H} = 0 \tag{21j}$$

Along the edge x=W-a it applies in analogy to the edge x=-a

$$\frac{\partial^2\Phi_s}{\partial x\partial y}|_{x=W-a} = 0 \tag{21k}$$

$$\frac{\partial^2 \Phi_s}{\partial y^2}\Big|_{x=W-a} = 0 \tag{21l}$$

This results in the boundary conditions

$$\frac{\partial \Phi_s}{\partial x}\Big|_{x=-a} = 0 \tag{22a}$$

$$\Phi_s|_{x=-a} = 0 \tag{22b}$$

$$\frac{\partial \Phi_s}{\partial y}\Big|_{y=H} = 0 \tag{22c}$$

$$\Phi_s|_{y=h} = \sigma_0\left(\frac{x^2}{2} + ax + \frac{a^2}{2}\right) \tag{22d}$$

$$\frac{\partial \Phi_s}{\partial x}\Big|_{x=W-a} = \sigma_0 W \tag{22e}$$

$$\Phi_s|_{x=W-a} = \frac{1}{2}\sigma_0 W^2 \tag{22f}$$

Figure 2 shows as the result the geometric function for different ratios a/W and H/W defined by

$$F = \frac{K_I}{\sigma_y\sqrt{\pi a}} \tag{23}$$

For comparison, data from [1] - based on computations by Gross and Srawley [2] - have been entered. Table 1 shows a comparison of the values determined here for H/W=2 with data taken from [1]. The agreement is very good. The maximum deviations from the solution proposed in the literature [1] are smaller than 1%.

a/W	Tension	Internal pressure	[1]
0.2	1.370	1.372	1.367
0.3	1.663	1.662	1.655
0.4	2.112	2.112	2.108
0.5	2.825	2.825	2.827
0.60	4.033	4.033	4.043
0.70	6.348	6.352	6.376
0.80	11.90	11.86	11.99

Table 1. Geometric function for the long plate (H/W=2) for tension

In fig.3 the influence is shown of the relative specimen length a/W for a/W=0.4. It is clearly visible that for H/W>1 no noticeable change in the geometric function F occurs any more and that hence the case H/W=1 reflects sufficiently well also plate strips infinite in length. In table 2 the geometric functions obtained for different H/W ratios have been compiled. Any intermediate values can be easily obtained by parabolic interpolation.
Figure 4 shows the influence of the number of considered terms of the series on the value of the geometric function F determined. A nearly constant value is attained from N=60 on. A clearly better convergence appears when the stress function is fitted to the boundary conditions as compared to the fitting of the stresses. For the geometric functions indicated in figs.2 and 3 always N=60 is used.

	a/W = 0.20	0.30	0.40	0.50	0.60	0.70
H/W = 0.35	1.743	2.264	2.852	3.581	4.635	6.678
0.5	1.487	1.848	2.324	3.009	4.149	6.393
0.75	1.381	1.680	2.133	2.841	4.040	6.355
1.00	1.372	1.662	2.113	2.825	4.033	6.354
1.25	1.370	1.662	2.112	2.825	4.033	6.354
1.50	1.370	1.662	2.112	2.825	4.033	6.354
2.00	1.370	1.663	2.112	2.825	4.033	6.352

Table 2. Influence of the plate length on the geometric function for tensile loading

An investigation of especially small cracks (e.g. a/W < 0.10) using the Boundary Collocation Method is not meaningful because in that case at the far distant fitting points - relative to the crack length - with r≫a the homogeneous stress field gets only little "disturbed". In the range of small values of a/W the plot determined for larger values of a/W can then be extrapolated to the value a/W = 0. Values for cracks occurring in the half-space of infinite extension - to which the case a/W corresponds - are provided with high accuracy by analytical methods.

3.2 The cracked plate with compression stresses acting on the crack surfaces

The crack loaded by constant pressure is, according to the principle of superposition of stress intensity factors, equivalent to the plate with crack loaded by tension of equal amount. The inter-comparison of the numerical results of both cases provides a measure of the accuracy of the method of collocation.
In the example under consideration the edge stresses are:

$$\sigma_x = 0 \quad , \quad \tau_{xy} = 0 \quad \text{für} \quad x = -a \tag{24a}$$

$$\sigma_y = 0 \quad , \quad \tau_{xy} = 0 \quad \text{für} \quad y = H \tag{24b}$$

$$\sigma_x = 0 \quad , \quad \tau_{xy} = 0 \quad \text{für} \quad x = W \tag{24c}$$

Integration of these stress conditions leads to the equivalent boundary conditions for the stress function:

$$\frac{\partial \Phi_s}{\partial x}\Big|_{x=-a} = -p_0 a \tag{25a}$$

$$\Phi_s|_{x=-a} = \frac{1}{2} p_0 a^2 \tag{25b}$$

$$\frac{\partial \Phi_s}{\partial y}\Big|_{y=H} = 0 \tag{25c}$$

$$\Phi_s|_{y=h} = -p_0 a\left(\frac{a}{2} + x\right) \tag{25d}$$

$$\frac{\partial \Phi_s}{\partial x}\Big|_{x=W-a} = -p_0 a \tag{25e}$$

$$\Phi_s|_{x=W-a} = -p_0 a\left(W - \frac{a}{2}\right) \tag{25f}$$

The geometric functions F obtained for the edge crack at constant compression stress loading of the crack faces has been entered in addition in table 1. The deviations from pure tensile loading are smaller than 0.4% and due to the fracture mechanics equivalents of both types of loading they are a measure of the accuracy of the numerical values. Thus, an increase in the number of series members of the expansion (13) taken into account (here N=60) does not seem necessary. It takes about 20s computer time to calculate a K-factor which time increases quadratically with the number of terms N. The results of the calculations of the stress intensity factors according to the BCM have been represented in fig.5a together with the literature data [1] , [5] , [6], The solid line corresponds to the geometric function tabulated in [1]. The values calculated by Benthem and Koiter [5] using the method of the asymptotic interpolation have been entered as dashed line; obviously, the accuracy of these values is particularly high close to the limit values a/W→0 and a/W→1. A numerical relation given by Tada [6]

$$F = 0.265(1-\alpha)^4 + \frac{0.857 + 0.265\alpha}{(1-\alpha)^{3/2}} \tag{26}$$

has been traced as a dotted-dashed line. However this formula does not express the correct (exactly known) derivative for a/W=0. The geometric functions calculated in that report can be represented by the numerical formula

$$F = 1.122\,\frac{0.026778\,(0.427103+\alpha)^{-2.73895} + 0.26514\,\alpha + 0.72475}{(1-\alpha)^{3/2}} \tag{27}$$

Figure 5b shows a comparison of the calculated points with the representation according to eq.(27).

3.3 *The plate subjected to bending load*

The stresses acting on the edges of the bent plate are:

$$\sigma_x = 0 \;,\; \tau_{xy} = 0 \quad \text{for} \quad x = -a \tag{28a}$$

$$\sigma_y = \sigma_0(1 - 2\,\frac{x+a}{W}) \;,\; \tau_{xy} = 0 \quad \text{für} \quad y = H \tag{28b}$$

$$\sigma_x = 0 \;,\; \tau_{xy} = 0 \quad \text{for} \quad x = W \tag{28c}$$

Expressed in terms of the stress function - similar to ref. [3] - the boundary conditions read:

$$\frac{\partial \Phi_s}{\partial x}\Big|_{x=-a} = 0 \tag{29a}$$

$$\Phi_s|_{x=-a} = 0 \tag{29b}$$

$$\frac{\partial \Phi_s}{\partial y}\Big|_{y=H} = 0 \tag{29c}$$

$$\Phi_s|_{y=H} = \sigma_0(-\frac{a^3}{3W} - \frac{a^2x}{W} - \frac{ax^2}{W} - \frac{x^3}{3W} + \frac{x^2}{2} + ax + \frac{a^2}{2}) \tag{29d}$$

$$\frac{\partial \Phi_s}{\partial x}\Big|_{x=W-a} = 0 \tag{29e}$$

$$\Phi_s|_{x=W-a} = \frac{1}{6}\,\sigma_0 W^2 \tag{29f}$$

The results of the computations have been represented in fig.6. Deviations are found up to 2% from the values in the table given in [1]. On the other hand, the agreement is excellent with the results proposed by Nisitani and Mori [4] (cited in [1]). The geometric functions calculated by those authors with the "Body Force Doublet Method" can be written

$$F = 1.122 - 1.121\alpha + 3.740\alpha^2 + 3.873\alpha^3 - 19.05\alpha^4 + 22.55\alpha^5 \quad (30)$$

Table 3 is a compilation of own results together with results from [1] and eq.(30).

a/W		[1]	[4], eq.(30)
0.10	1.048		1.049
0.20	1.058	1.035	1.055
0.3	1.126	1.098	1.127
0.4	1.261	1.234	1.263
0.50	1.497	1.475	1.495
0.60	1.913	1.898	1.917
0.70	2.709	2.716	2.714

Table 3. The geometric function for the long plate (H/W=2) under bending load

3.4 The weight function for mode I loading

Stress intensity factors for cracks exposed to any loading can be calculated using the **weight functions method**. If a stress distribution $\sigma(x)$ acts on the crack surfaces of a one-dimensional crack of depth a , the effective stress intensity factor K_I is given by

$$K_I = \sigma^* \sqrt{\pi a}\, F = \int_0^a h(x,a)\sigma(x)\, dx \quad (31)$$

where σ^* is a characteristic stress value of the stress distribution $\sigma(x)$, e.g. the stress acting near the plate surface. The weight functions h(x,a) used in (31) are known for important types of crack. They can be calculated from the crack opening displacement field of any reference load case - normally chosen with σ = constant - using

$$h(x,a) = \frac{E'}{K_{Ir}} \frac{\partial}{\partial a} v_r(x,a) \quad (32)$$

The subscript r denotes the reference load case. For the module E' we must introduce E in case of plane stress and $E/(1-\nu^2)$ in case of plane strain. In order to be able to determine the weight function for a crack/component configuration we have to determine the crack opening displacement field of the reference load case as well as the related stress intensity factor. It is proposed to determine in this report the weight function for the edge cracked plate (see fig.1) from stress collocation computations and to compare it with solutions indicated in the literature.

3.5 The crack opening displacement field for the reference load case

The displacements u and v can be calculated from the radial strains ε_r and tangential strains ε_φ. The following relation holds:

$$\varepsilon_r = \frac{\partial u}{\partial r} \quad (33)$$

$$\varepsilon_\varphi = \frac{u}{r} + \frac{1}{r} \frac{\partial v}{\partial \varphi} \quad (34)$$

From the Hook law written in a general version

$$\varepsilon_r = m\sigma_r - n\sigma_\varphi \tag{35a}$$

$$\varepsilon_\varphi = m\sigma_\varphi - n\sigma_r \tag{35b}$$

with

$$m = \frac{1}{E} \quad , \quad n = \frac{\nu}{E} \qquad \text{for plane stress}$$

$$m = \frac{1-\nu^2}{E} \quad , \quad n = \frac{\nu(1+\nu)}{E} \qquad \text{for plane strain}$$

and the stress components given by the stress function Φ

$$\sigma_r = \frac{1}{r}\frac{\partial\Phi}{\partial r} + \frac{1}{r^2}\frac{\partial^2\Phi}{\partial\varphi^2}$$

$$\sigma_\varphi = \frac{\partial^2\Phi}{\partial r^2} \tag{36}$$

$$\tau_{r\varphi} = \frac{1}{r^2}\frac{\partial\Phi}{\partial\varphi} - \frac{1}{r}\frac{\partial^2\Phi}{\partial r\partial\varphi}$$

we obtain the following system of equations describing the displacements

$$\frac{\partial u}{\partial r} = \frac{m}{r}\frac{\partial\Phi}{\partial r} + \frac{m}{r^2}\frac{\partial^2\Phi}{\partial\varphi^2} - n\frac{\partial^2\Phi}{\partial r^2} \tag{37a}$$

$$\frac{u}{r} + \frac{1}{r}\frac{\partial v}{\partial\varphi} = m\frac{\partial^2\Phi}{\partial r^2} - \frac{n}{r}\frac{\partial\Phi}{\partial r} - \frac{n}{r^2}\frac{\partial^2\Phi}{\partial\varphi^2} \tag{37b}$$

The integration of this system of differential equations leads to

$$v = -m\int\int\frac{1}{r}\frac{\partial\Phi}{\partial r}\,dr d\varphi - m\int\int\frac{1}{r^2}\frac{\partial^2\Phi}{\partial\varphi^2}\,dr d\varphi + m\int\frac{\partial^2\Phi}{\partial r^2}\,d\varphi - \frac{n}{r}\frac{\partial\Phi}{\partial\varphi} \tag{38}$$

After introduction of the stress function - with the coefficients A, A^* determined by the BCM -

$$\Phi_s = \sum_{n=0}^{\infty} r^{n+3/2} A_n \left[\cos(n+3/2)\varphi - \frac{n+3/2}{n-1/2}\cos(n-1/2)\varphi \right]$$

$$+ \sum_{n=0}^{\infty} r^{n+2} A_n^* [\cos(n+2)\varphi - \cos n\varphi] \tag{39}$$

we obtain for the crack opening displacements on account of $\varphi = \pi$

$$v_{\varphi=\pi} = m\sum_{n=0}^{\infty} A_n r^{n+1/2}\, 4\,\frac{n+3/2}{n-1/2}\,(-1)^{n+1} \tag{40}$$

Figure 7 shows the crack opening displacements for cracks of different depths as normalized plots. For comparison, the approximative crack opening displacements have been entered in addition which had been obtained in [7] and [8] on the basis of the reference stress intensity factor, the conditions of self-consistence, and the requirement of vanishing bending on the surface. The agreement is very good for relative crack depths a/W≤0.7 with maximum deviations of about 1%. For a/W=0.8 the maximum deviations increase to approx. 3%. As the representation in an approximation relies on a polynomial expansion with only three terms in $r^{n+1/2}$ it is evident that the

real crack contour can be satisfied only by averaging over the total crack depth. According to these deviations, also deviations in the weight function can be anticipated in case that the latter are determined by the method of approximation and not by crack opening displacement fields determined in a direct manner.

3.6 *Determination of the weight function*

Since up to a/W=0.7 the crack opening displacement fields determined by approximation according to [7] [8]are not identical with the values determined according to the BCM - the deviation being 1% - the weight function indicated in [8] can be used for a/W≤0.7. It is contained in the Annex as fitted formula.
Starting from the crack opening displacement fields determined according to eq.(40) the weight function h(x,a) will now be newly calculated for a/W>0.5. Table 4 shows as a basis for the calculations the crack opening displacements for several values a/W and ξ/a ($\xi = x + a$; see fig.1) in the form suited for interpolations

$$v = \frac{\sigma}{E'} a \frac{\sqrt{1-\xi/a}}{(1-a/W)^{5/2}} \cdot f\left(\frac{\xi}{a}, \frac{a}{W}\right) \tag{41}$$

This leads to the derivation of the crack opening displacements with respect to the crack length. The function values needed for numerical differentiation of the function f have been interpolated from the values given in table 4 using bicubic splines. With the help of eqs.(27) and (32) the values of the weight function are obtained which have been compiled in table 5. The values so obtained have been entered in fig.8 together with the weight function given in [8]. Likewise, the weight function solution according to Bückner [9] has been represented with a range of validity a/W<0.6 as well as the solution proposed by Kaya [10]. In the range a/W<0.6 all weight functions are nearly identical.

ξ/a	a/W=0.5	0.6	0.7	0.75	0.8
0.0	1.7464	1.6779	1.5838	1.5152	1.4225
0.2	1.6805	1.5880	1.4739	1.3985	1.3029
0.4	1.6193	1.4959	1.3555	1.2710	1.1705
0.6	1.5567	1.3962	1.2233	1.1268	1.0193
0.8	1.4888	1.2841	1.0706	0.9577	0.8386

Table 4. Normalized crack opening displacements f(ξ/a,x/W) according to eq.(41)

Table 6 shows the weight function values from table 5 in a representation which lends itself easily to interpolation

$$h = \sqrt{\frac{2}{\pi a}} \frac{g(\xi/a, a/W)}{\sqrt{1-\xi/a}\,(1-a/W)^{3/2}} \tag{42}$$

In order to make possible interpolations up to a/W→1 the solution known from analysis for a/W=1 (slotted half-space with remaining dam) [6]

$$h = \frac{2}{\sqrt{\pi a}} 3.52 \frac{1-\xi/a}{(1-a/W)^{3/2}} \tag{43}$$

has been incorporated in this table. The values for $\xi/a = 1$ result from the crack tip field (near-field) which is exclusively determined by the stress intensity factor

$$v_{nah} = \sqrt{8}\,\frac{\sigma}{E'} F \tag{44}$$

Using eq.(32) this results in the weight function applicable to the crack tip zone

$$h = \sqrt{\frac{8}{\pi a}}\left[\frac{\xi/a}{2\sqrt{1-\xi/a}} + (1+\frac{a}{F}\frac{\partial F}{\partial a})\sqrt{1-\xi/a}\right] \tag{45}$$

and especially for $\xi/a \to 1$

$$h = \sqrt{\frac{2}{\pi a}}\,\frac{\xi/a}{\sqrt{1-\xi/a}} \tag{46}$$

independent of a/W .

a/W	$\xi/a=0.0$	0.2	0.4	0.6	0.8	0.9
0.5	9.270	8.139	7.032	6.000	5.249	5.401
0.6	13.605	11.618	9.661	7.787	6.170	5.811
0.7	21.54	18.17	14.80	11.46	8.263	
0.75	28.88	24.12	19.37	14.63	10.01	
0.8	41.14	34.06	26.96	19.87	12.86	

Table 5. Weight functions h(ξ/a,a/W) from crack opening displacement fields

a/W	$\xi/a=0.0$	0.2	0.4	0.6	0.8	0.9	1.0
0.0	1.834	1.624	1.440	1.273	1.128	1.060	1.000
0.1	1.796	1.575	1.379	1.190	1.007	0.928	0.8538
0.2	1.933	1.650	1.402	1.160	0.920	0.815	0.7155
0.3	2.195	1.830	1.488	1.155	0.852	0.715	0.5857
0.4	2.527	2.050	1.600	1.172	0.793	0.620	0.4648
0.5	2.907	2.295	1.725	1.195	0.738	0.535	0.3536
0.6	3.298	2.548	1.850	1.230	0.693	0.450	0.2530
0.7	3.711	2.800	1.975	1.250	0.637	0.370	0.1643
0.75	3.918	2.927	2.036	1.260	0.607	0.330	0.1250
0.8	4.125	3.054	2.094	1.260	0.577	0.297	0.0894
1.0	4.978	3.562	2.314	1.259	0.445	0.157	0.0000

Table 6. Weight function in a normalized representation g(ξ/a,a/W) according to eq.(43)

Using the data from table 6 the weight function can be expressed within $\pm 1\%$ accuracy by the approximation formula

$$h = \sqrt{\frac{2}{\pi a}}\,\frac{1}{\sqrt{1-\xi/a}\,(1-a/W)^{3/2}}\left[(1-\frac{a}{W})^{3/2} + \sum A_{\nu\mu}(1-\xi/a)^{\nu+1}(\frac{a}{W})^{\mu}\right] \tag{47}$$

The related coefficients are:

$$A_{00} = 0.4980 \quad A_{01} = 2.4463 \quad A_{02} = 0.0700 \quad A_{03} = 1.3187 \quad A_{04} = -3.067$$

$$A_{10} = 0.54165 \quad A_{11} = -5.0806 \quad A_{12} = 24.3447 \quad A_{13} = -32.7208 \quad A_{14} = 18.1214$$

$$A_{20} = -0.19277 \quad A_{21} = 2.55863 \quad A_{22} = -12.6415 \quad A_{23} = 19.7630 \quad A_{24} = -10.9860$$

4. Edge cracked plate under mode II loading

To be able to evaluate fracture toughness measurements knowledge is required of the stress intensity factor solution applicable to the load case chosen. Besides in the mode I loading studied thoroughly, the interest is growing in mode II and mixed mode loadings. Here the continuous surface crack under constant shear loading τ_0 will be examined as the reference load case for weight function application.
The following relations hold for stresses acting on the specimen edge

$$\sigma_x = 0 \quad , \quad \tau_{xy} = 0 \quad \text{für} \quad x = -a \tag{48a}$$

$$\sigma_y = 0 \quad , \quad \tau_{xy} = 0 \quad \text{für} \quad y = H \tag{48b}$$

$$\sigma_x = 0 \quad , \quad \tau_{xy} = 0 \quad \text{für} \quad x = W \tag{48c}$$

Integration of these stress conditions gives the equivalent boundary conditions for the stress function:

$$\frac{\partial \Phi_a}{\partial x}\Big|_{x=-a} = 0 \tag{49a}$$

$$\Phi_a|_{x=-a} = \tau_0 a y \tag{49b}$$

$$\frac{\partial \Phi_a}{\partial y}\Big|_{y=H} = \tau_0 a \tag{49c}$$

$$\Phi_a|_{y=h} = \tau_0 a H \tag{49d}$$

$$\frac{\partial \Phi_a}{\partial x}\Big|_{x=W-a} = 0 \tag{49e}$$

$$\Phi_a|_{x=W-a} = \tau_0 a y \tag{49f}$$

The geometric functions F obtained for the edge crack at constant shear stress loading of the crack faces have been entered in table 7. The results of the computations have been entered in fig.9. The solution obtained by Tada [6] from the asymptotic interpolation according to the method by Benthem und Koiter [5] has been represented in addition.

$$F_{II} = \frac{1.122 - 0.561a/W + 0.085(a/W)^2 + 0.180(a/W)^3}{\sqrt{1 - a/W}} \tag{50}$$

With the formula above the two exactly known limit cases of the straight continuous surface crack in the half-space (a/W→0) and of the slotted half-space with remaining dam (a/W→1) are interpolated, with the derivation $dF_{II}/d(a/W)$ for the limit case a/W→0 known in addition by a suitable polynomial and, obviously, its accuracy is maximum near a/W=0 and a/W=1. Deviations up to approx. 1.5% from the formula indicated in [6] are found.
The geometric functions determined in that study can be represented analytically by the relation

$$F_{II} = \frac{1.122 - 0.561a/W - 0.20(a/W)^2 + 0.89115(a/W)^3 - 0.42609(a/W)^4}{\sqrt{1 - a/W}} \tag{51}$$

4.1 Determination of the mode II weight function

The computation of stress intensity factors for cracks loaded by **shear stresses** can be performed using the weight function for mode II loadings. If the stress distribution $\tau(x)$ acts on the crack surfaces of the one-dimensional crack the mode II stress intensity factor is expressed by

$$K_{II} = \tau^* \sqrt{\pi a}\, F = \int_0^a h_{II}(x,a)\tau(x)\, dx \tag{52}$$

where τ^* is a characteristic stress value of the stress distribution $\tau(x)$. The weight function h_{II} can be calculated by

$$h_{II}(x,a) = \frac{E'}{K_{IIr}} \frac{\partial}{\partial a} u_r(x,a) \tag{53}$$

4.2 The crack opening displacement field for the reference load case

The displacements u and v are described by eqs.(33) and (34). Using eq.(33)

$$\varepsilon_r = \frac{\partial u}{\partial r}$$

and the Hooke law - eq.(35) - we obtain especially for $\varphi = \pi$ - since in this case σ_φ -

$$\frac{\partial u}{\partial r}\Big|_{\varphi=\pi} = m\sigma_r \tag{54}$$

The integration of eq.(54) gives for the reference case of constant shear stress on the crack surface using eq.(5a)

$$u_r|_{\varphi=\pi} = 4m \sum_{n=0}^{\infty} (-1)^n B_n r^{n+1/2} \tag{55}$$

The crack opening displacements determined according to eq.(55) were compared with a solution proposed in the literature [6] for the special case r = a, i.e. for crack opening on the surface. Clear deviations were found. By verifying the derivation of the solution indicated in [6] an error in [6] was detected. The correct derivation - and likewise an intercomparison of the crack opening - have been described in more detail in the Annex.

4.3 Determination of the mode II weight function

The weight function can be determined with eq.(53) from the crack opening displacements determined by eq.(55). Very accurate solutions are available for the limit cases a/W→0 and a/W→1 [6]. Together with these limit cases the values of the weight function for discrete values of a/W and ξ/a (see fig.1) entered in table 8 yield in the normalized representation

$$h = \sqrt{\frac{2}{\pi a}}\, \frac{g(\xi/a, a/W)}{\sqrt{1-\xi/a}\,\sqrt{1-a/W}} \tag{56}$$

In fig.10 the weight function for cracks of different depths is shown in a normalized representation. From the data in table 8 the weight function for each value of a/W and ξ/a can be obtained by parabolic interpolation. The IMSL-routine IBCIEU is suited for this purpose.
An analytical approximative representation for a/W≤0.9 can be described by

$$h = \sqrt{\frac{2}{\pi a}}\, \frac{1}{\sqrt{1-\xi/a}\,(1-a/W)^{1/2}} \left[\left(1 - \frac{a}{W}\right)^{1/2} + \sum A_{\nu\mu} (1-\xi/a)^{\nu+1} \left(\frac{a}{W}\right)^{\mu} \right] \tag{57}$$

The related coefficients $A_{\nu\mu}$ are entered in table 9.

4.4 *Stress intensity factors for short plates*

The influence of the height H on the geometric function F_{II} is represented in table 10. For small values of H/W (H/W≤0.4) and a/W<0.8 a simple relation becomes obvious by plotting the F_{II}-data versus a/H. The result is shown in fig.11 . A unique relation occurs which can be described by the simple relation

$$F_{II} \simeq \left[1.684(a/H)^2 + 1.1215^4\right]^{1/4} \tag{58}$$

a/W	F_{II}	Gl.(9)
0.2	1.128	1.134
0.25	1.133	1.143
0.3	1.143	1.155
0.4	1.178	1.191
0.50	1.239	1.252
0.60	1.345	1.351
0.70	1.523	1.520
0.80	1.846	1.833
0.85	2.129	2.110
0.90	2.620	2.584

Table 7. Geometric function for the long plate with constant shear stresses acting on the crack faces

a/W	$\xi/a=0.0$	0.2	0.4	0.6	0.8	0.9	1.0
0.0	1.834	1.624	1.440	1.273	1.128	1.061	1.000
0.2	1.662	1.488	1.311	1.146	1.007	0.947	0.894
0.4	1.543	1.382	1.209	1.048	0.902	0.834	0.775
0.6	1.556	1.382	1.199	1.009	0.813	0.728	0.632
0.8	1.690	1.502	1.289	1.048	0.778	0.615	0.447
0.9	1.766	1.570	1.356	1.096	0.791	0.573	0.316
1.0	1.834	1.641	1.421	1.160	0.820	0.580	0.000

Table 8. Mode II weight function in a normalized representation g(ξ/a,a/W) according to eq.(56)

	$\mu=0$	1	2	3
$\nu=0$	0.59250	0.08077	-2.93912	6.06686
1	0.15745	-1.83168	11.7816	-14.599
2	0.21108	2.8108	-14.701	15.329
3	-0.12416	-1.6465	6.69787	-6.15696

Table 9. Coefficients of the weight function according to eq.(57)

H/W	a/W=0.1	0.2	0.3	0.4	0.5	0.7	0.9
0.025	2.369	3.272	3.977	4.582	5.092	6.022	6.826
0.05	1.762	2.373	2.858	3.272	3.644	4.292	4.845
0.1	1.366	1.763	2.090	2.375	2.629	3.075	3.479
0.2	1.172	1.366	1.575	1.763	1.934	2.237	2.772
0.4	1.122	1.174	1.261	1.366	1.474	1.707	2.611
0.5			1.205	1.282	1.371	1.615	
0.6			1.174	1.232	1.309	1.567	0.000
0.75			1.152	1.194	1.262	1.536	0.000

Table 10. Geometric function for the short plate

5. Applications of the two weight functions

5.1 *The edge-notched beam in asymmetric 4-point bending*

As an example of application the weight functions h_I *and* h_{II} are used to calculate the stress intensity factors of edge-notched beams in asymmetric bending-arrangements (fig.12). Such a test configuration is of interest for the determination of the fracture toughness K_{IIc} of ceramic materials. In this case the geometric functions F_I and F_{II} are defined by

$$K_I = \frac{P}{Wt}\left(1-\frac{d}{L}\right)\sqrt{\pi a}\,F_I \quad , \quad K_{II} = \frac{P}{Wt}\left(1-\frac{d}{L}\right)\sqrt{\pi a}\,F_{II} \tag{59}$$

The non-symmetrically loaded (unnotched) 4-point bending bar was studied by Filon [11] who derived an analytical solution for the stress state. The axial stresses σ_x, normal to the crack, are

$$\begin{aligned}\sigma_x = &-\frac{2P}{L}\sum_{n=1}^{\infty}\cos md\,\frac{\sinh mW/2 - mW/2\cosh mW/2}{mW+\sinh mW}\cos mx\cosh my\\ &-\frac{2P}{L}\sum_{n=1}^{\infty}\cos md\,\frac{my\sinh mW/2}{mW+\sinh mW}\cos mx\sinh my\\ &-\frac{2P}{L}\sum_{n=1}^{\infty}\sin md\,\frac{\cosh mW/2 - mW/2\sinh mW/2}{\sinh mW - mW}\sin mx\sinh my\\ &-\frac{2P}{L}\sum_{n=1}^{\infty}\sin md\,\frac{my\cosh mW/2}{\sinh mW - mW}\sin mx\cosh my\end{aligned} \tag{60}$$

with $m = n\pi/L$, and the shear stresses τ are given by

$$\begin{aligned}\tau = &\frac{2P}{L}\sum_{n=1}^{\infty}\cos md\,\frac{mW/2\cosh mW/2}{mW+\sinh mW}\sin mx\sinh my\\ &-\frac{2P}{L}\sum_{n=1}^{\infty}\cos md\,\frac{my\sinh mW/2}{mW+\sinh mW}\sin mx\cosh my\\ &-\frac{2P}{L}\sum_{n=1}^{\infty}\sin md\,\frac{mW/2\sinh mW/2}{\sinh mW - mW}\cos mx\cosh my\\ &\frac{2P}{L}\sum_{n=1}^{\infty}\sin md\,\frac{my\cosh mW/2}{\sinh mW - mW}\cos mx\sinh my\end{aligned} \tag{61}$$

An illustration of the shear stresses τ along the line x=0 is given in Fig.13 and the normal stresses σ_x are represented in Fig.14. The numerical calculations were carried out with at least 500 terms in the center ($y\simeq 0$) increasing to 10000 terms for the outer regions $y\rightarrow\pm W/2$. Based on the stress fields $\sigma_x(y)$, $\tau(y)$, the stress intensity factors for mode-I and mode-II result,

$$K_I = \int_0^a h_I(\eta/a,a/W)\,\sigma_x\,d\eta \quad , \quad K_{II} = \int_0^a h_{II}(\eta/a,a/W)\,\tau\,d\eta \tag{62}$$

$$\eta = \frac{W}{2} - y \tag{63}$$

5.1.1 The long beam without eccentricity

The stress intensity factors (expressed by the geometric functions) are listed in tables 11 and 12 for L/W=5 and various a/W- and d/W-values. From these results any other combination can be obtained easily by application of bicubic splines.

	d/W=0.25	0.300	0.375	0.500	0.625
a/W=0.1	0.3746	0.3428	0.3318	0.3450	0.3599
0.2	0.7881	0.7180	0.6719	0.6633	0.6741
0.3	1.0374	0.9933	0.9560	0.9399	0.9431
0.4	1.1858	1.1819	1.1753	1.1702	1.1695
0.5	1.3120	1.3380	1.3579	1.3661	1.3641
0.6	1.4674	1.5079	1.5387	1.5507	1.5472
0.7	1.6948	1.7318	1.7553	1.7600	1.7547
0.8	2.053	2.0687	2.073	2.0684	2.0635
0.9	2.7563	2.7545	2.7505	2.7467	2.7452

Table 11. Geometric function for mode II

	d/W=0.25	0.300	0.375	0.500	0.625
a/W=0.1	0.2615	0.3695	0.4241	0.3841	0.2918
0.2	-0.0038	0.1129	0.2110	0.2448	0.2060
0.3	-0.0307	0.0447	0.1184	0.1580	0.1410
0.4	0.0024	0.0483	0.0904	0.1098	0.09534
0.5	0.0407	0.0672	0.0842	0.0806	0.06268
0.6	0.0716	0.0808	0.0771	0.0566	0.03706
0.7	0.0855	0.0769	0.0581	0.03198	0.0164
0.8	0.0641	0.0460	0.0271	0.0106	0.00359
0.9	-0.0048	-0.0002	0.0077	0.01406	0.0138

Table 12. Geometric function for mode I

Figure 15 shows a comparison of the results of weight functions with the FE-results given in [12]. For this case especially L/W=2.5 was chosen. As can be seen from tables 11 and 12 the geometric function F_{II} is approximately independent of the value of d/W in the range $0.375 \leq d/W \leq 625$. An analytical approximation can be given by

$$F_{II} = 3.9204\alpha - 5.1295\alpha^2 + 14.4566\alpha^3 - 26.2916\alpha^4 + 17.073\alpha^5 \quad , \quad \alpha = a/W \tag{64}$$

5.1.2 The influence of an eccentricity

In order to evaluate tests with small misalignments, where the crack is not located exactly between the inner rollers with an eccentricity Δx , stress intensity factors were calculated for $\Delta x = \pm 0.2d$ and d/W=0.5 in addition. By interpolation of the values in table 13 the influence of the eccentricity can be taken into account.

	$\Delta x/d$ =-0.2	0.	+0.2
0.1	0.3544	0.3450	0.3355
0.2	0.7081	0.6633	0.6296
0.4	1.2320	1.1702	1.1110
0.6	1.5747	1.5507	1.5170
0.8	2.0667	2.0584	2.0700

Table 13. Geometric function for eccentric crack location (mode II)

5.1.3 The influence of the specimen length

The geometric function F_{II} was computed for several values of the ratio L/W. The results are shown in table 14 for the case d/W=0.5. It is obvious that the specimen length exerts only an insignificant influence.

	L/W=1.25	2.50	3.75	5.00	7.50
a/W=0.1	0.3293	0.3411	0.3438	0.3450	0.3462
0.2	0.6485	0.6596	0.6621	0.6633	0.6644
0.4	1.1700	1.1702	1.1703	1.1702	1.1703
0.6	1.5575	1.5524	1.5513	1.5507	1.5503
0.8	2.0735	2.0697	2.0689	2.0684	2.0682
0.9	2.7480	2.7471	2.7470	2.7467	2.7468

Table 14. Geometric function (mode II) for different ratios L/W

5.1.4 Recommendation for mode-II experiments

For mode-II experiments it is recommended to use specimens with $0.4<a/W<0.6$ since the mode-I stress intensity factor is very small in this range. The remaining mode-I portion guarantees a crack opening and avoids friction effects between the two crack surfaces. For d/W $0.35 \leq d/W \leq 0.625$ should be chosen since in this range the geometric function F_{II} is nearly independent of d/W. The specimen lengths should be L/W>2 to obtain a geometric function F_{II} which is nearly independent of the specimen length.

5.2 *Stress intensity factor and compliance in 3-point bending tests*

Three-point bending tests are usually carried out to determine subcritical crack growth of macro-cracks in static bending tests and to determine the R-curve effect of ceramics. Therefore, the stress intensity factors are necessary as well as the compliance.
The geometric function F defined by

$$K_I = \sigma_0 F \sqrt{\pi a} \quad , \quad \sigma_0 = \frac{3}{2} \frac{PL}{W^2 B} \tag{65}$$

has been determined by Brown and Srawley [2], [3] for 3-point bending tests with L/W=4 and 8 with the Boundary-Collocation-Method (BCM). In this section the stress intensity factor and the

compliance of bending bars are analyzed in a wide range of L/W using the weight function method. The aim is, to provide data which allow to evaluate tests with arbitrary geometry (L/W≥2).

5.2.1 Stress distribution

The symmetrically supported 3-point bending bar (fig.16) was studied by Filon [11] who derived

$$\begin{aligned}\sigma_x = & -\frac{3yPL}{2W^3} - \frac{4P}{L}\sum_{n=1}^{\infty}\frac{\sinh mW/2 - mW/2\cosh mW/2}{mW+\sinh mW}\cos mx\cosh my \\ & -\frac{4P}{L}\sum_{n=1}^{\infty}\frac{my\sinh mW/2}{mW+\sinh mW}\cos mx\sinh my \\ & -\frac{4P}{L}\sum_{n=0}^{\infty}\frac{\cosh MW/2 - MW/2\sinh MW/2}{\sinh MW - MW}\cos Mx\sinh My \\ & -\frac{4P}{L}\sum_{n=0}^{\infty}\frac{My\cosh MW/2}{\sinh MW - MW}\cos Mx\cosh My\end{aligned} \tag{66}$$

with $m = 2n\pi/L$, and $M = (2n+1)\pi/L$.
An illustration of the resulting stresses σ_x along the line x=0 is given in Fig.17.

5.2.2 Stress intensity factors

The stress intensity factors -expressed by the geometric function F and illustrated in fig.18 - were fitted by

$$F = \frac{1}{(1-\alpha)^{3/2}}\left[0.3738\alpha + (1-\alpha)(A_0 + A_1\alpha + A_2\alpha^2 + A_3\alpha^3 + A_4\alpha^4)\right] \quad , \quad \alpha = a/W \tag{67}$$

The coefficients $A_0....A_4$ are listed in table 15 for different values of L/W. From these results the coefficients for any other L/W≥2 can be obtained easily by application of bicubic splines.

	A_0	A_1	A_2	A_3	A_4
L/W=2	1.0426	-2.2336	3.9625	-3.3469	1.0121
4	1.0697	-2.0120	3.4980	-2.9588	0.8756
8	1.0941	-1.9105	3.1971	-2.6356	0.7445
16	1.1063	-1.8598	3.0477	-2.4759	0.6801
32	1.1130	-1.8420	3.0018	-2.4385	0.6690
∞	1.1200	-1.8286	2.9734	-2.4268	0.6706

Table 15. Constants for eq.(67)

A representation by polynomials reads

$$A_\mu = A_{\mu 0} + A_{\mu 1}W/L + A_{\mu 2}(W/L)^2 + A_{\mu 3}(W/L)^3 + A_{\mu 4}(W/L)^4 \quad , \quad \mu = 0....4 \tag{68}$$

with the coefficients listed in table 16.

	$A_{\mu 0}$	$A_{\mu 1}$	$A_{\mu 2}$	$A_{\mu 3}$	$A_{\mu 4}$
$\mu=0$	1.1200	-0.2387	0.4317	-1.7351	2.4145
$\mu=1$	-1.8288	-0.2573	-4.9847	16.9047	-18.2883
$\mu=2$	2.9741	0.2706	18.6767	-60.4912	59.9239
$\mu=3$	-2.4280	0.5627	-27.3447	87.7078	-85.2405
$\mu=4$	0.6712	-0.5184	13.5837	-43.5421	42.3503

Table 16. Coefficients for eq.(68)

5.2.3 Compliance

The compliance of a bending bar with the crack size a consists of the compliance of the uncracked bar C_0 and the portion ΔC caused by the crack. The total compliance is then given by

$$C = C_0 + \Delta C \tag{69}$$

with

$$C_0 = \frac{L^2}{W^2 BE}\left[\frac{L}{4W} + \frac{(1+\nu)W}{2L}\right] \tag{70}$$

(E = Youngs modulus, ν = Poisson ratio, B = specimen width), and

$$\Delta C = \frac{9}{2}\frac{L^2\pi}{W^2 EB}\int_0^{\alpha} F^2\,\alpha'\,d\alpha' \tag{71}$$

The result of the numerical evaluation of eq.(71) can be expressed as

$$\Delta C = \frac{9}{2}\frac{L^2}{W^2 EB}\left(\frac{\alpha}{1-\alpha}\right)^2\sum_{\mu=0}^{5} B_\mu \alpha^\mu \tag{72}$$

with the coefficients of table 17. Figure 19 shows the compliance in a normalized representation.

	B_0	B_1	B_2	B_3	B_4	B_5
L/W = 2	1.7046	-6.251	13.924	-18.867	14.073	-4.3928
4	1.7950	-5.9908	12.452	-16.161	11.609	-3.508
8	1.8787	-5.9556	11.742	-14.669	10.200	-2.9972
16	1.9210	-5.9329	11.368	-13.894	9.4753	-2.7354
32	1.9424	-5.9220	11.185	-13.524	9.1344	-2.6138
∞	1.9638	-5.9091	10.991	-13.128	8.7669	-2.4818

Table 17. Constants for eq.(72)

The data of table 17 can be fitted by

$$B_\mu = B_{\mu 0} + B_{\mu 1} W/L + B_{\mu 2}(W/L)^2 + B_{\mu 3}(W/L)^3 \quad , \quad \mu = 0....5 \tag{73}$$

with the coefficients listed in table 18.

	$B_{\mu 0}$	$B_{\mu 1}$	$B_{\mu 2}$	$B_{\mu 3}$
$\mu=0$	1.9634	-0.6473	-0.4645	1.4479
$\mu=1$	-5.9080	-0.5307	1.8855	-4.3890
$\mu=2$	10.9909	6.2296	-2.3368	3.2163
$\mu=3$	-13.130	-12.356	0.08942	3.3477
$\mu=4$	8.7702	11.3087	1.7797	-6.3733
$\mu=5$	-2.4832	-4.0318	-0.9616	2.7738

Table 18. Coefficients for eq.(73)

5.3 The 3-point bending test with eccentric notch

In a three-point bending test with a notched bar under asymmetric load (fig.20) the geometric functions F_I , F_{II} may be defined by

$$K_I = \sigma_0 F_I \sqrt{\pi a} \quad , \; K_{II} = \sigma_0 F_{II} \sqrt{\pi a} \; , \; \sigma_0 = \frac{3}{2} \frac{PL}{W^2 B} \tag{74}$$

In order to determine the mixed-mode stress intensity factors the weight function method is applied in this section.

5.3.1 Stress distribution

The symmetrically supported 3-point bending bar (fig.1) was studied by Filon [11] who derived an analytical solution for the stress state. The stress components necessary for fracture-mechanical calculations read

$$\begin{aligned} \sigma_x = & -\frac{12yPL}{W^3} - \frac{4P}{L}\sum_{n=1}^{\infty} \frac{\sinh mW/2 - mW/2 \cosh mW/2}{mW + \sinh mW} \cos mx \cosh my \\ & - \frac{4P}{L}\sum_{n=1}^{\infty} \frac{my \sinh mW/2}{mW + \sinh mW} \cos mx \sinh my \\ & - \frac{4P}{L}\sum_{n=0}^{\infty} \frac{\cosh MW/2 - MW/2 \sinh MW/2}{\sinh MW - MW} \cos Mx \sinh My \\ & - \frac{4P}{L}\sum_{n=0}^{\infty} \frac{My \cosh MW/2}{\sinh MW - MW} \cos Mx \cosh My \end{aligned} \tag{75}$$

$$\tau = \frac{4P}{L}\sum_{n=1}^{\infty}\frac{mW/2\cosh mW/2}{mW+\sinh mW}\sin mx\sinh my$$
$$-\frac{4P}{L}\sum_{n=1}^{\infty}\frac{my\sinh mW/2}{mW+\sinh mW}\sin mx\cosh my$$
$$+\frac{4P}{L}\sum_{n=0}^{\infty}\frac{MW/2\sinh MW/2}{\sinh MW-MW}\sin Mx\cosh My \qquad (76)$$
$$-\frac{4P}{L}\sum_{n=0}^{\infty}\frac{My\cosh MW/2}{\sinh MW-MW}\sin Mx\sinh My$$

with $m = 2n\pi/L$, and $M = (2n+1)\pi/L$.
An illustration of the resulting stresses σ_x and τ is given in figs.21 and 22.

5.3.2 Stress intensity factors

The mode-I and mode-II stress intensity factors were calculated by introducing eqs.(75) and (76) in eqs.(77). The results are expressed by the geometric functions F_I, F_{II} and compiled in tables 19-24. From these results the coefficients for any other L/W≥2 can be obtained easily by application of bicubic splines (e.g. IMSL-bicubic-spline routine IBCIEU).

	2d/L=0.	0.2	0.4	0.6	0.7	0.8	0.9
a/W=0.	1.0426	0.9757	0.8171	0.6462	0.5747	0.5348	0.5692
0.1	0.8067	0.7560	0.6292	0.4663	0.3647	0.2089	-0.1222
0.2	0.6583	0.6145	0.5032	0.3521	0.2564	0.1345	-0.0011
0.3	0.5655	0.5240	0.4210	0.2864	0.2094	0.1274	0.0497
0.4	0.5065	0.4648	0.3664	0.2468	0.1837	0.1206	0.0601
0.5	0.4674	0.4235	0.3276	0.2194	0.1648	0.1106	0.0584
0.6	0.4390	0.3911	0.2972	0.1982	0.1490	0.1005	0.0521
0.7	0.4164	0.3627	0.2719	0.1809	0.1359	0.0911	0.0467
0.8	0.3977	0.3362	0.2510	0.1672	0.1254	0.0837	0.0421

Table 19. Geometric function for mode-I at L/W=2

	2d/L=0.2	0.4	0.6	0.7	0.8	0.9
a/W=0.1	0.0320	0.0481	0.0529	0.0642	0.1164	0.3687
0.2	0.0557	0.0868	0.1069	0.1359	0.2146	0.3893
0.3	0.0743	0.1167	0.1453	0.1750	0.2315	0.3093
0.4	0.0899	0.1378	0.1649	0.1858	0.2172	0.2522
0.5	0.1041	0.1513	0.1709	0.1825	0.1979	0.2116
0.6	0.1183	0.1585	0.1689	0.1740	0.1802	0.1841
0.7	0.1333	0.1598	0.1628	0.1641	0.1660	0.1662
0.8	0.1462	0.1551	0.1545	0.1546	0.1549	0.1534

Table 20. Geometric function for mode-II at L/W=2

	2d/L=0.2	0.4	0.6	0.7	0.8	0.9
a/W=0.	0.9450	0.7187	0.5058	0.4223	0.3596	0.3466
a/W=0.1	0.7480	0.5750	0.3998	0.3188	0.2267	0.0397
0.2	0.6179	0.4755	0.3252	0.2496	0.1604	0.0344
0.3	0.5315	0.4067	0.2745	0.2070	0.1331	0.0533
0.4	0.4720	0.3581	0.2398	0.1801	0.1187	0.0571
0.5	0.4280	0.3220	0.2148	0.1615	0.1079	0.0547
0.6	0.3924	0.2935	0.1956	0.1470	0.0986	0.0504
0.7	0.3615	0.2700	0.1799	0.1351	0.0904	0.0458
0.8	0.3348	0.2506	0.1670	0.1253	0.0836	0.0419

Table 21. Geometric function for mode-I at L/W=3

	2d/L=0.2	0.4	0.6	0.7	0.8	0.9
a/W=0.1	0.0328	0.0406	0.0348	0.0324	0.0402	0.1282
0.2	0.0553	0.0696	0.0638	0.0649	0.0871	0.1912
0.3	0.0712	0.0895	0.0856	0.0895	0.1131	0.1779
0.4	0.0827	0.1018	0.0995	0.1036	0.1206	0.1550
0.5	0.0915	0.1081	0.1063	0.1091	0.1189	0.1358
0.6	0.0983	0.1097	0.1080	0.1093	0.1139	0.1208
0.7	0.1028	0.1076	0.1061	0.1065	0.1081	0.1107
0.8	0.1030	0.1030	0.1022	0.1022	0.1025	0.1030

Table 22. Geometric function for mode-II at L/W=3

	2d/L=0.2	0.4	0.6	0.7	0.8	0.9
a/W=0.	0.9324	0.6859	0.4640	0.3712	0.2961	0.2648
a/W=0.1	0.7450	0.5540	0.3741	0.2938	0.2158	0.0445
0.2	0.6187	0.4625	0.3111	0.2399	0.1651	0.0607
0.3	0.5330	0.3989	0.2673	0.2034	0.1364	0.0597
0.4	0.4729	0.3536	0.2362	0.1785	0.1194	0.0583
0.5	0.4278	0.3196	0.2132	0.1605	0.1075	0.0545
0.6	0.3914	0.2924	0.1949	0.1465	0.0981	0.0502
0.7	0.3604	0.2697	0.1798	0.1349	0.0902	0.0458
0.8	0.3343	0.2505	0.1670	0.1253	0.0836	0.0422

Table 23. Geometric function for mode-I at L/W=4

	2d/L=0.2	0.4	0.6	0.7	0.8	0.9
a/W=0.1	0.0295	0.0316	0.0272	0.0244	0.0238	0.0567
0.2	0.0497	0.0543	0.0481	0.0454	0.0499	0.1049
0.3	0.0633	0.0693	0.0632	0.0616	0.0692	0.1131
0.4	0.0722	0.0781	0.0730	0.0723	0.0793	0.1062
0.5	0.0777	0.0820	0.0783	0.0779	0.0827	0.0971
0.6	0.0805	0.0824	0.0800	0.0798	0.0822	0.0888
0.7	0.0805	0.0804	0.0792	0.0790	0.0799	0.0823
0.8	0.0778	0.0770	0.0765	0.0764	0.0766	0.0772

Table 24. Geometric function for mode-II at L/W=4

6. Literature

[1] Y.Murakami et al, Stress intensity factors handbook, Pergamon Press 1986.

[2] B. Gross, J.E. Srawley, W.F. Brown, NASA, Technical Note, D-2395, 1965.

[3] B. Gross, J.E. Srawley, NASA, Technical Note, D-2603, 1965.

[4] H. Nisitani, K. Mori, Tech. Reports of the Kyushu Univ. Vol 58 (1985),751-755 (zitiert in [1])

[5] J.P. Benthem. W.T. Koiter, Asymptotic approximations to crack problems, in: Mechanics of Fracture I, ed. G.C. Sih, Noordhoff International Publ., Leyden, 1973.

[6] H. Tada, "The stress analysis of cracks handbook", Del. Research Corporation (1986).

[7] T. Fett, C. Mattheck, D. Munz , Engng. Fract. Mech. **27**(1987),697-715.

[8] T. Fett, A weight function for the single edge crack based on approximative displacement fields, Theor. and Appl. Fract. Mech. **8**(1987),169-172.

[9] H. Bueckner, Field singularities and related integral representations, in: Mechanics of Fracture I - Methods of Analysis and Solution of Crack Problems, ed. by G.C. Sih, Noordhoff, Leyden (1979).

[10] A.C. Kaya, F. Erdogan, Stress intensity factors on COD in an orthotropic strip, Int. J. Fracture **16**(1980),171-190.

[11] L.N.G. Filon,"On an approximate solution for the bending of a beam of rectangular cross-section under any system of load, with special reference to points of concentrated or discontinuous loading", Phil. Trans., A, 201(1903),63-155.

[12] A. Otsuka, T. Tohgo, T. Kiba, S. Yamada, "Mode-II fatigue crack growth characteristics and mechanism in aluminium alloy 7N01-T4 weldments under mode-II loading", Advances in Fracture Research,Proc. ICF 6, 3 ,Pergamon,(1984),pp.1671-1678.

7. Annex

7.1 Weight function from approximative crack opening displacements

The weight function determined from approximative crack opening displacements in [8] with $\rho = \xi/a$ reads

$$h(x, a) = \sqrt{\frac{2}{\pi a}} \frac{1}{\sqrt{1-\rho}} [1 + A_1(1-\rho) + A_2(1-\rho)^2 + A_3(1-\rho)^3] \qquad (A1)$$

with the coefficients obtained by fitting

$$A_1 = \frac{0.4523 + 1.1690\frac{a}{t} + 8.5078(\frac{a}{t})^2 - 13.6598(\frac{a}{t})^3 + 4.4806(\frac{a}{t})^4}{(1-a/t)^{3/2}} \qquad (A2)$$

$$A_2 = \frac{0.7017 - 2.2134\frac{a}{t} + 2.7344(\frac{a}{t})^2 + 4.6756(\frac{a}{t})^3 - 6.0185(\frac{a}{t})^4}{(1-a/t)^{5/2}} \qquad (A3)$$

$$A_3 = \frac{-0.3102 + 0.9970\frac{a}{t} - 0.5156(\frac{a}{t})^2 - 2.0149(\frac{a}{t})^3 - 1.8843(\frac{a}{t})^4}{(1-a/t)^{5/2}} \qquad (A4)$$

As appears from a comparison with the weight function determined according to the BCM, the solution indicated here yields sufficiently accurate values up to a/W=0.75.

7.2 Comparison of the crack opening displacement field under mode II loading with a solution proposed in the literature

In [6] the crack opening displacement directly at the surface was indicated for the case of the edge crack loaded with constant shear stresses using to the method of Paris (see [6] Annex B).

$$\delta_{II} = \frac{4\tau a}{E'} \cdot U_1(\alpha) \quad , \quad \alpha = a/W \qquad (A5)$$

where the function U_1 has been represented by

$$U_1 = -0.184 - 0.637\alpha - 0.129\alpha^2 + 0.026\alpha^3 + 0.028\alpha^4 + 0.008\alpha^5 - \frac{1.644}{\alpha}\ln(1-\alpha) \qquad (A6)$$

This solution is shown in fig. A1. In addition, the results obtained by use of eq.(55) are entered. The deviations of the two solutions occur well beyond the accuracies of the two methods.
If K_{IP} means the stress intensity factor caused by a (continuous) loading P and K_{IQ} means the stress intensity factor caused by a point load Q at the crack mouth ($\xi=0$ in fig.1) the crack opening displacement for $\xi=0$ is obtained as follows

$$\delta_{\xi=0} = \frac{2}{E'} \int_0^a K_{IP} \frac{\partial K_{IQ}}{\partial Q}\, da \qquad (A7)$$

With the stress intensity factor given in [6]

$$K_{IQ} = \frac{2Q}{\sqrt{\pi a}} \frac{1.3 - 0.65\alpha + 0.37\alpha^2 + 0.28\alpha^3}{\sqrt{1-\alpha}} \qquad (A8)$$

and

$$K_{IP} = \tau\sqrt{\pi a}\ \frac{1.122 - 0.561\alpha + 0.085\alpha^2 + 0.18\alpha^3}{\sqrt{1-\alpha}} \qquad (A9)$$

Introducing (A8) and (A9) into eq.(A7) after elementary integration leads to

$$U_1 = 0.3848 - 0.5369\alpha - 0.06117\alpha^2 + 0.02546\alpha^3 - 0.02816\alpha^4 - 0.0084\alpha^5 - \frac{1.0738}{\alpha}\ln(1-\alpha) \quad (A10)$$

This relation - controlled by numerical integration of eq.(A7) - is likewise entered in fig.A1. Within the accuracy of both methods it agrees with the dependence resulting from eq.(55).

8. Figures

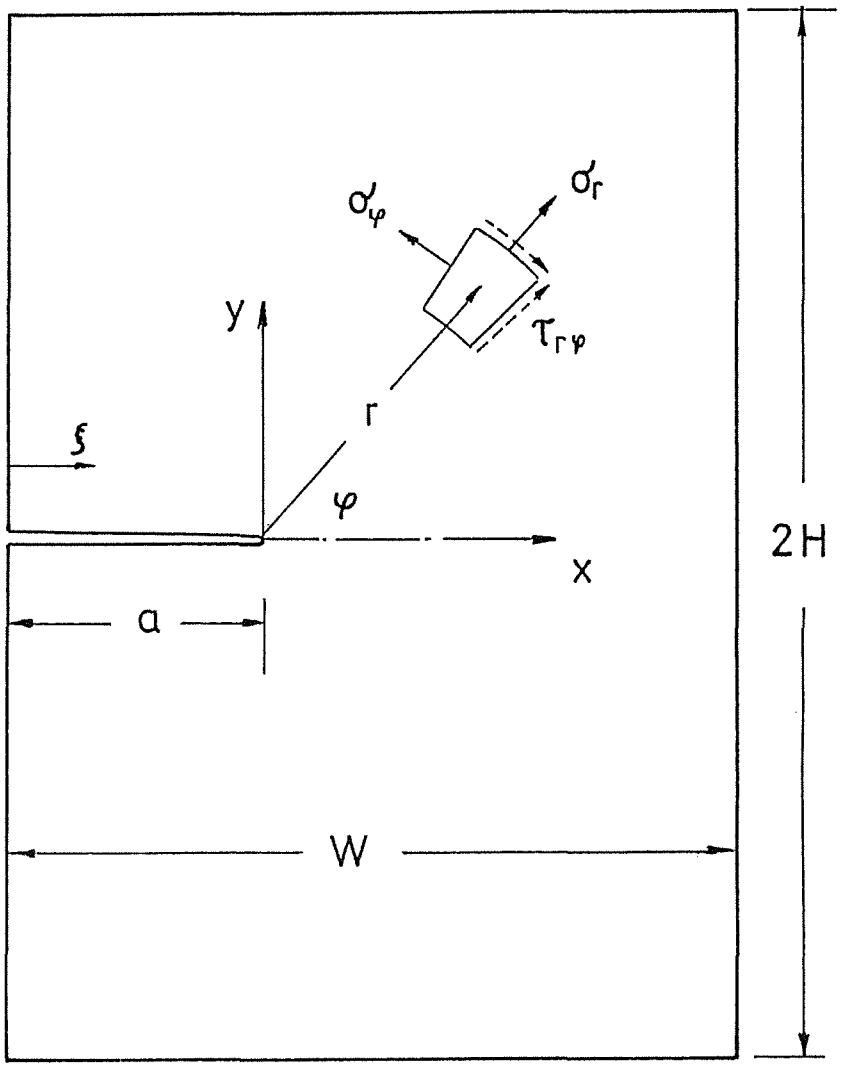

Fig.1

Coordinate system and stresses ahead of the crack tip.

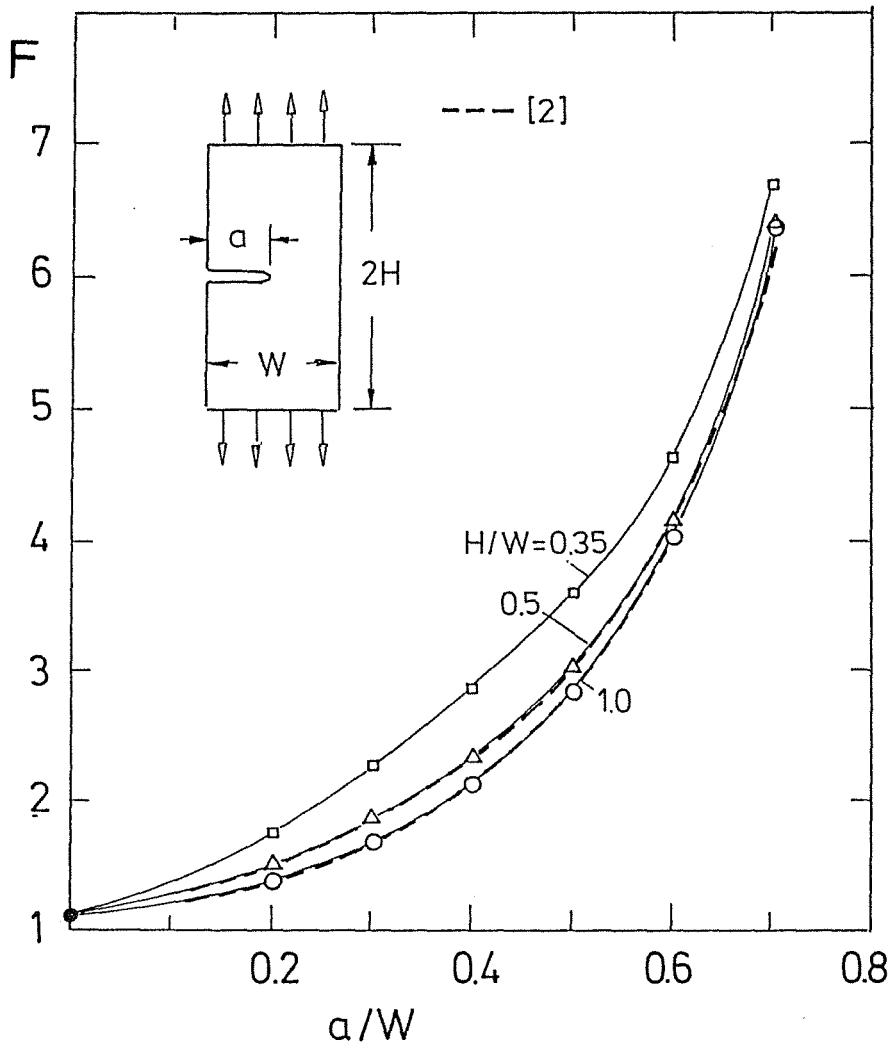

Fig.2

Geometric function of the "edge-crack" subjected to tensile stress.

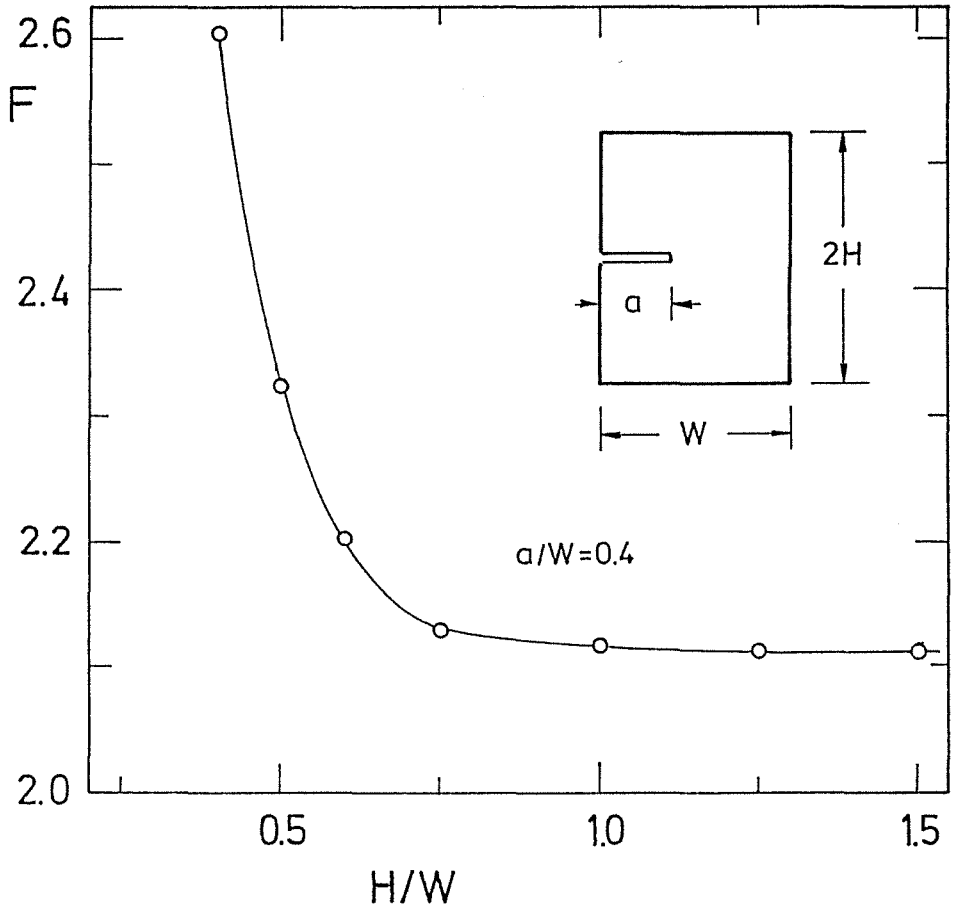

Fig.3

Influence of the specimen length 2H on the geometric function under tensile loading.

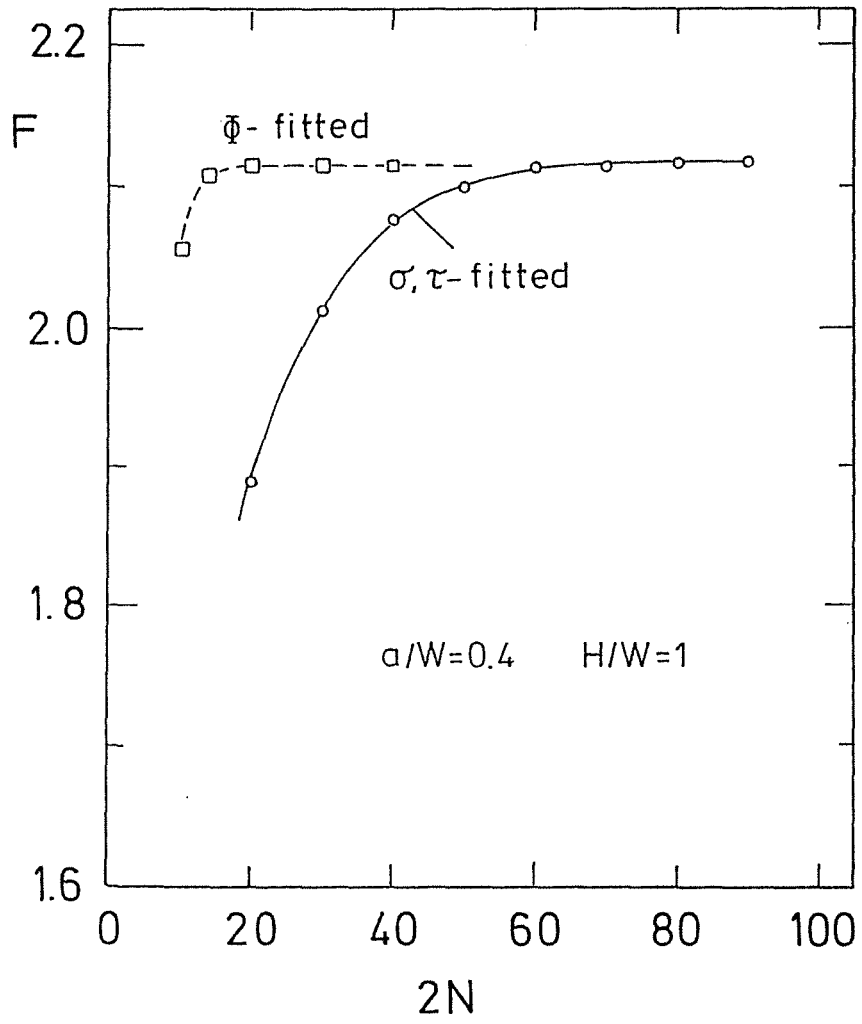

Fig.4

On the convergence of the Boundary Collocation Method after fitting of the stress function and the stresses acting on the edge, resp.

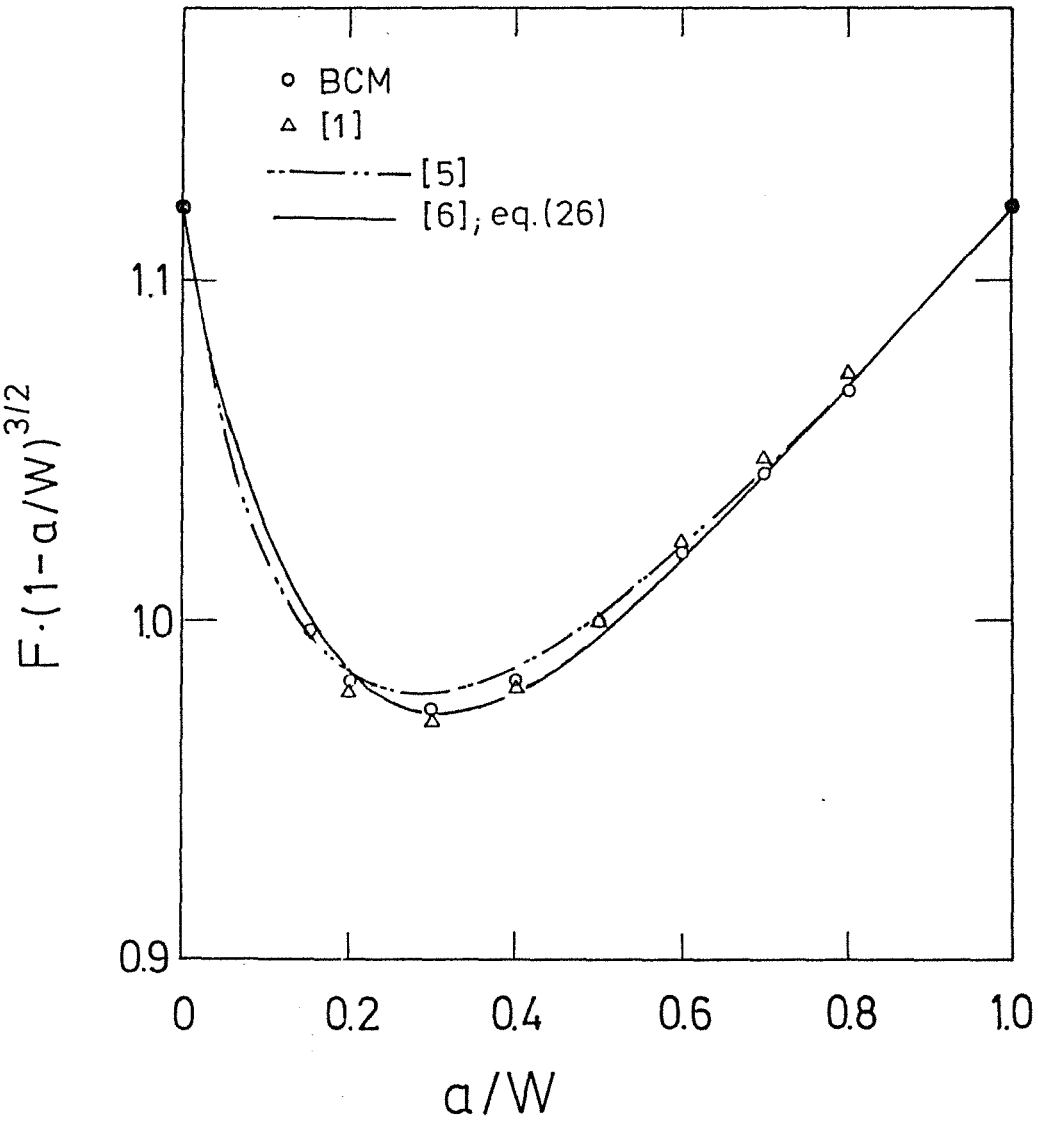

Fig.5a

Comparison of the results obtained with the BCM with data from the literature.

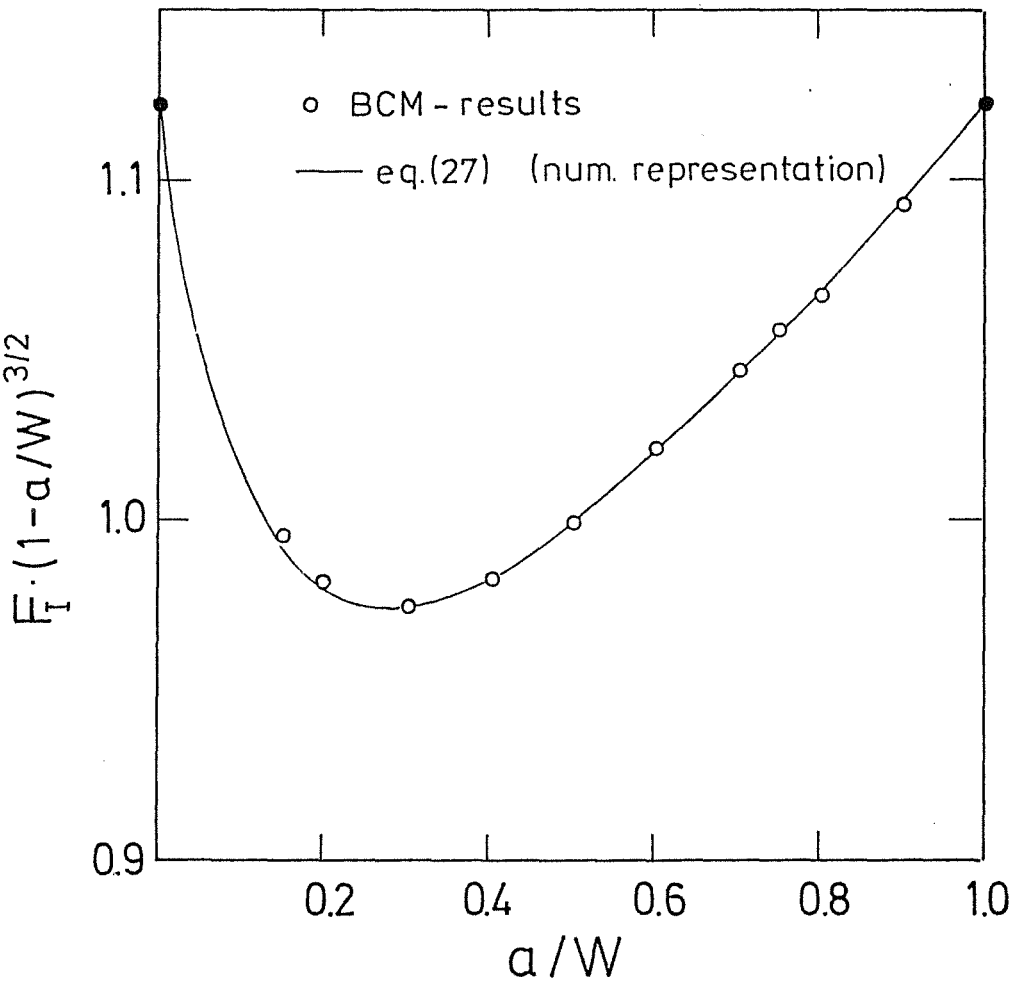

Fig.5b

Own results and their analytical representation by eq.(27).

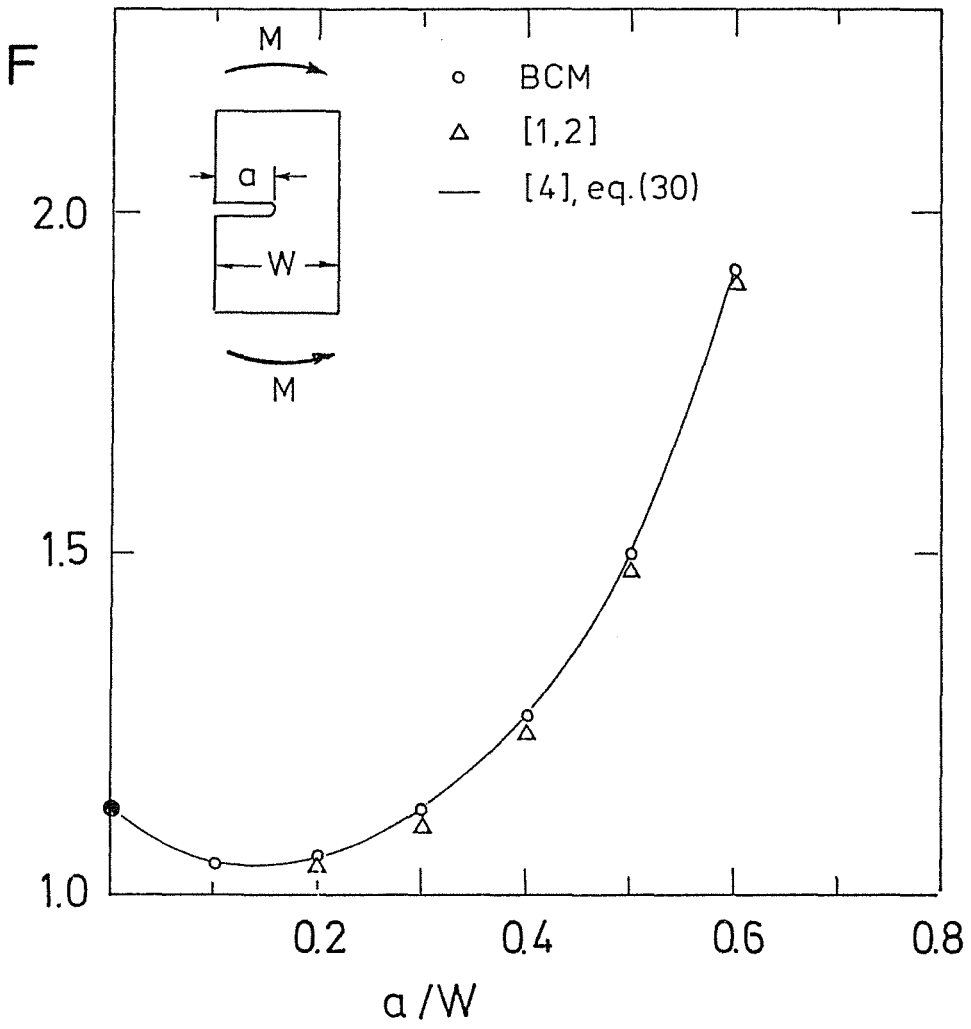

Fig.6

Comparison of the geometric function F for the case of pure bending with a solution taken from a table in [1].

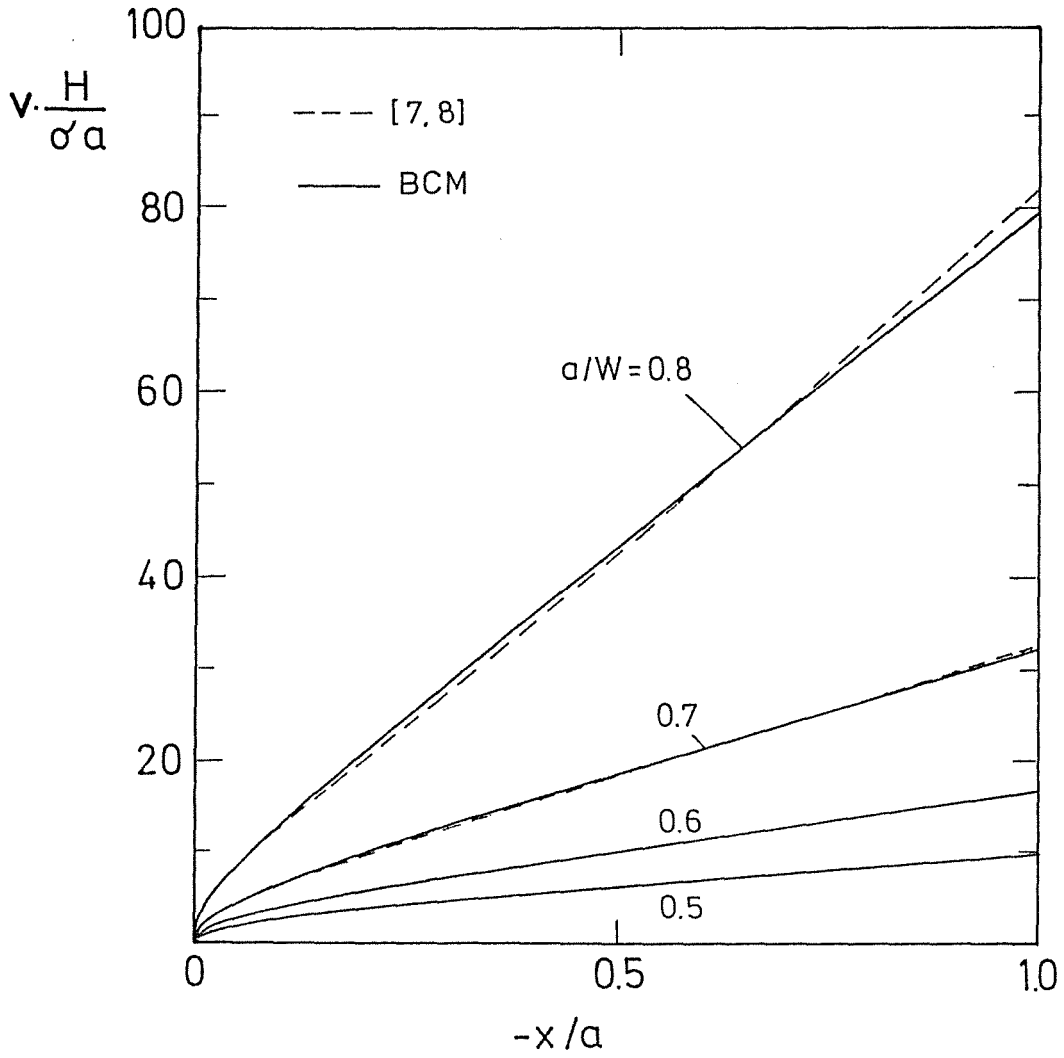

Fig.7

Crack opening displacements according to the BCM, compared with crack profiles obtained by an approximation method indicated in [8].

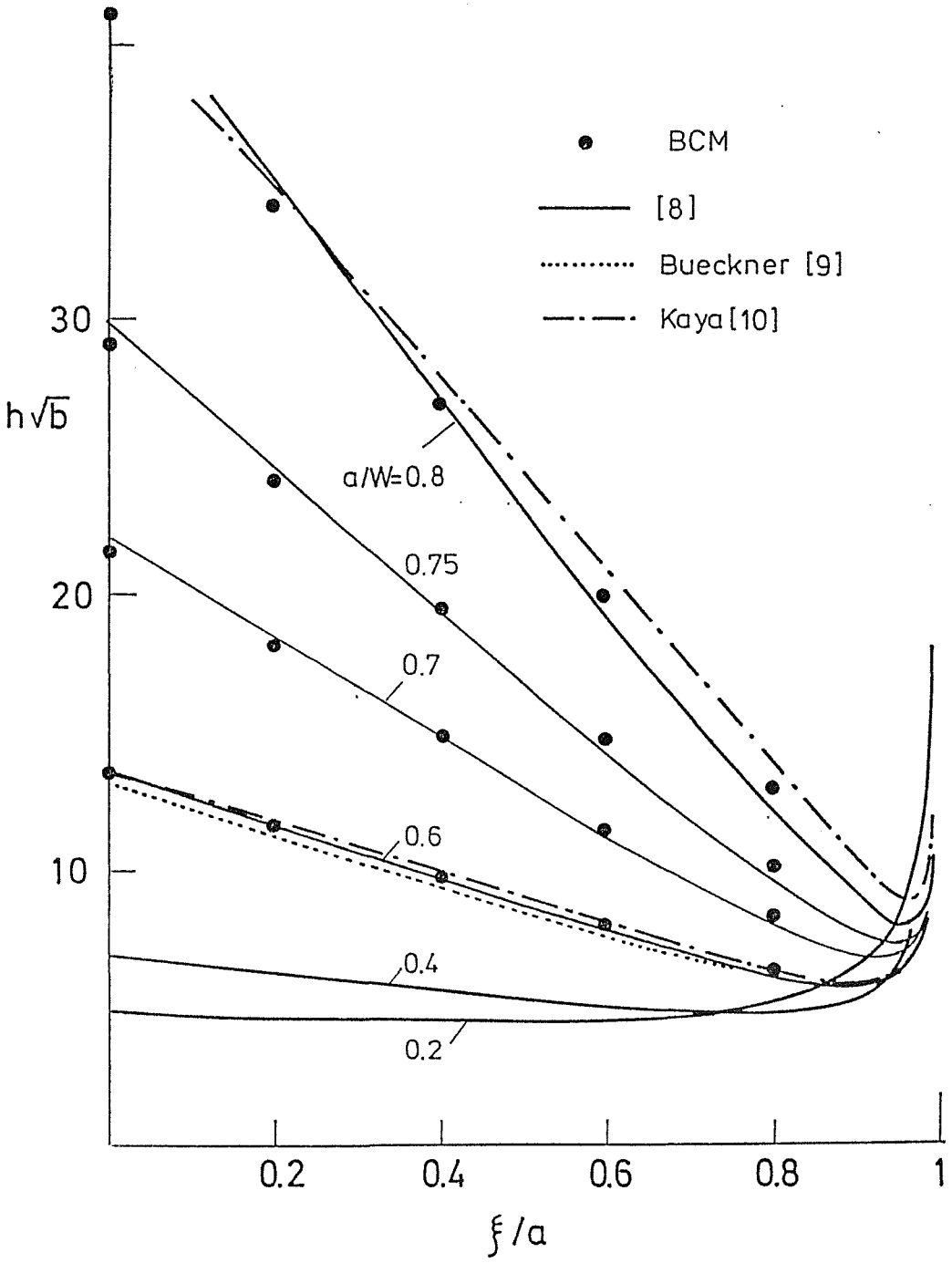

Fig.8

Values of the weight function of the edge cracked plate, compared with solutions indicated in the literature.

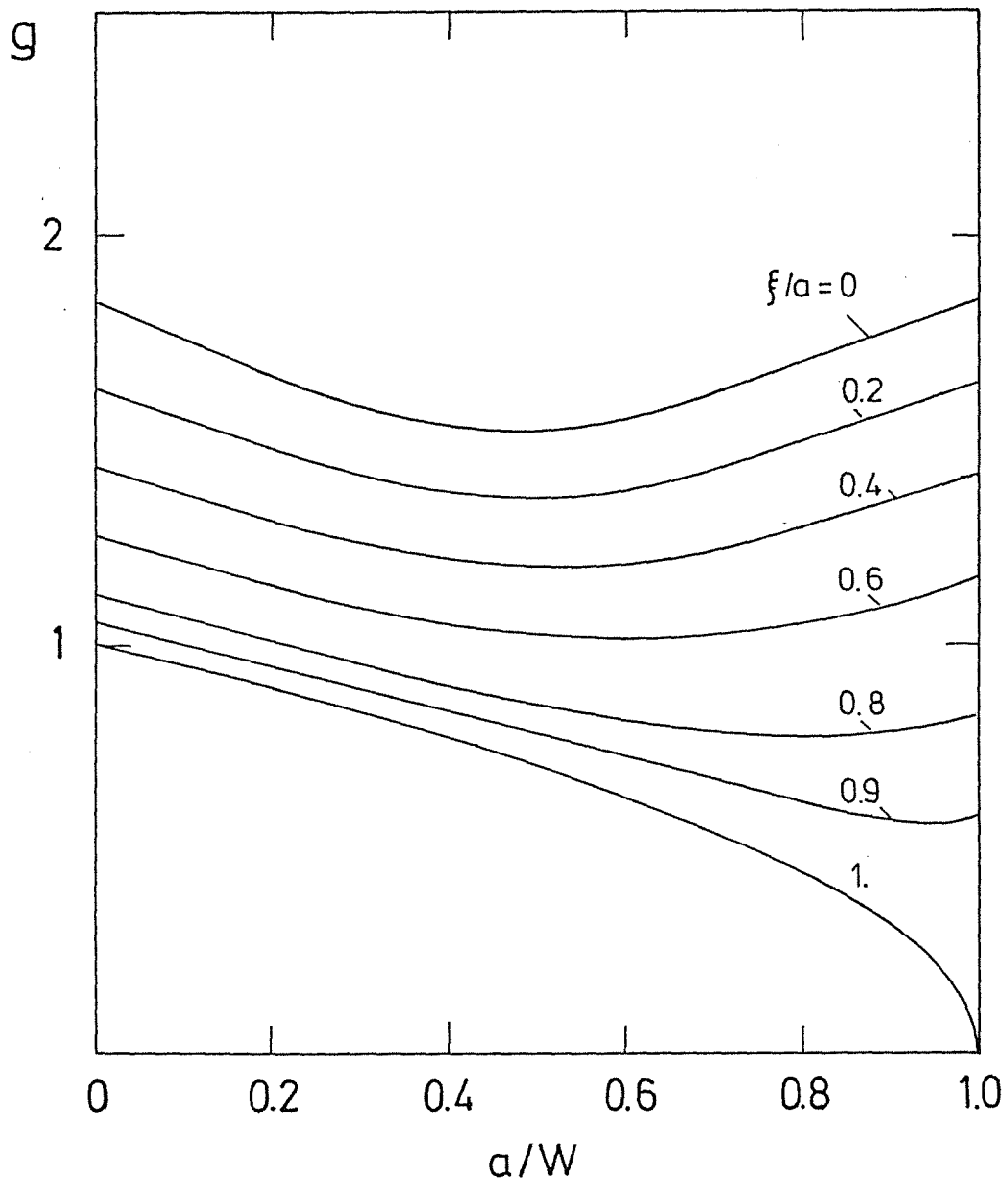

Fig.10

Weight function $h_{//}$ in a normalized representation $g(\xi/a, a/W)$ according to eq.(56).

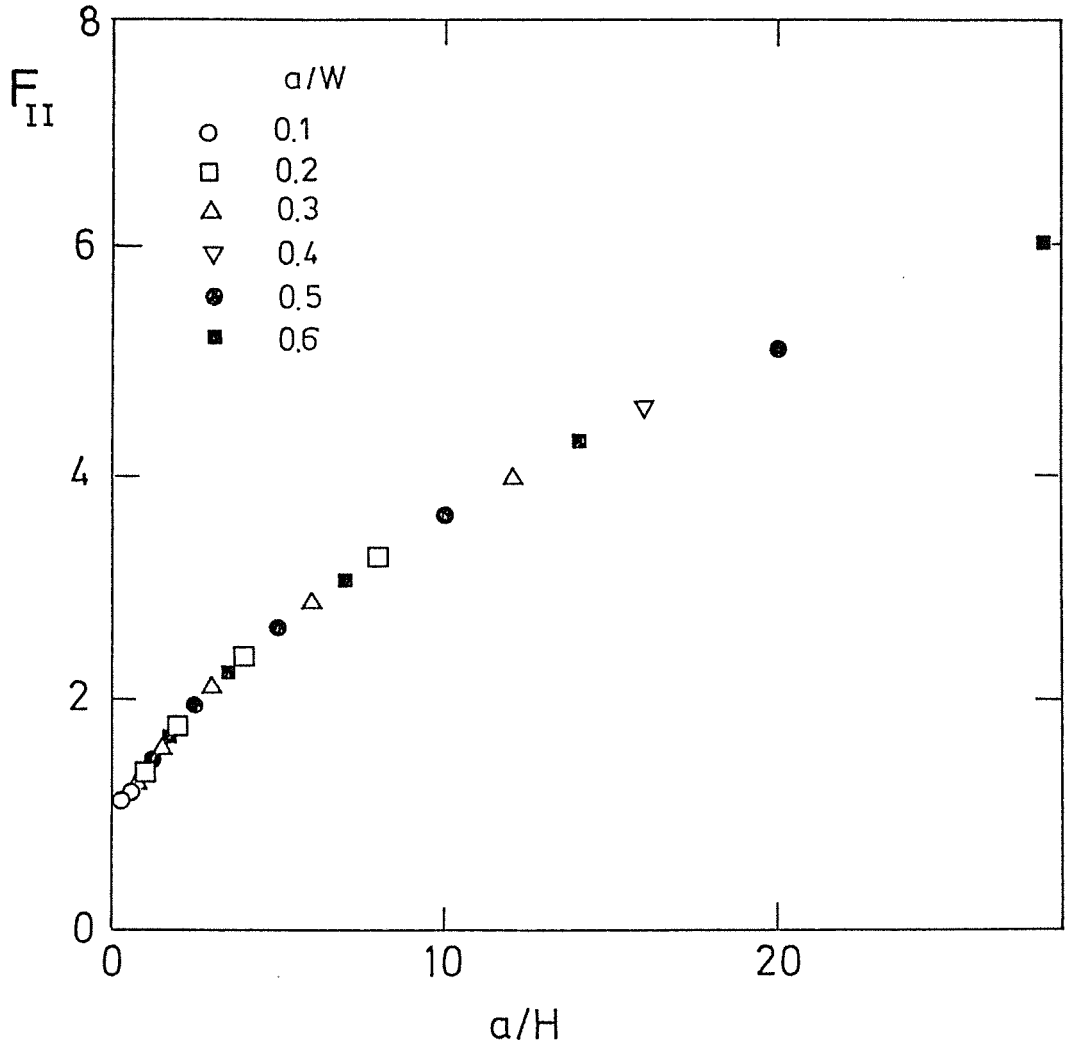

Fig.11

Geometric function F_{II} for small values of H/W.

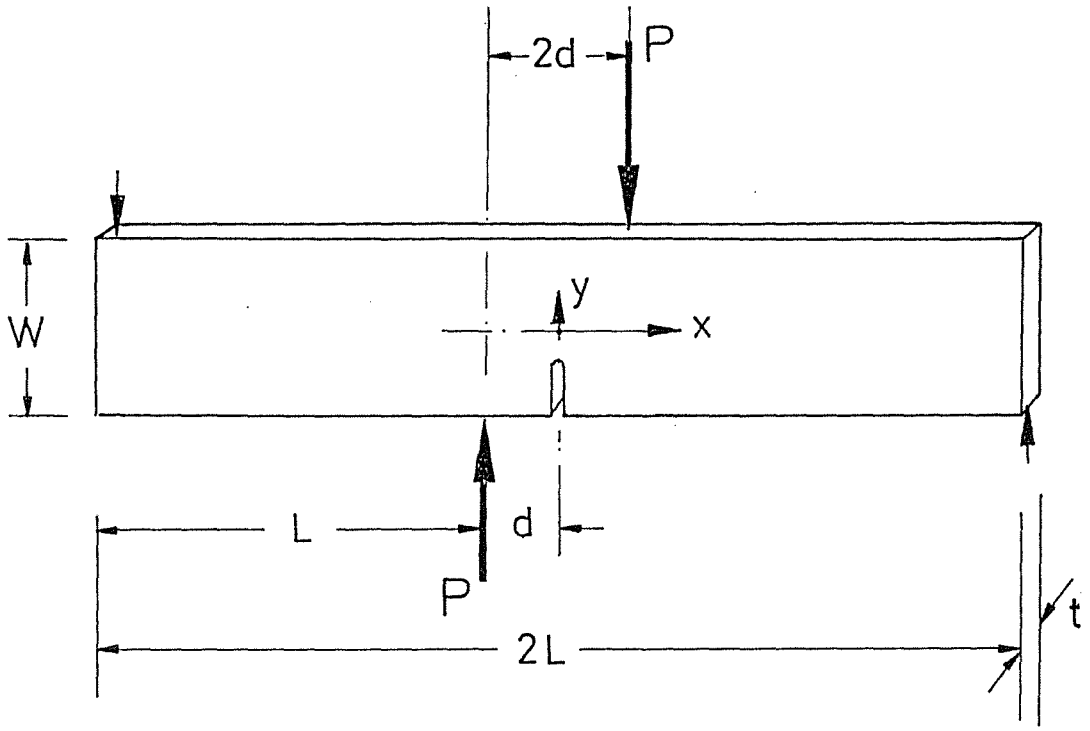

Fig.12

Edge-notched bending bar in an asymmetrical bending test.

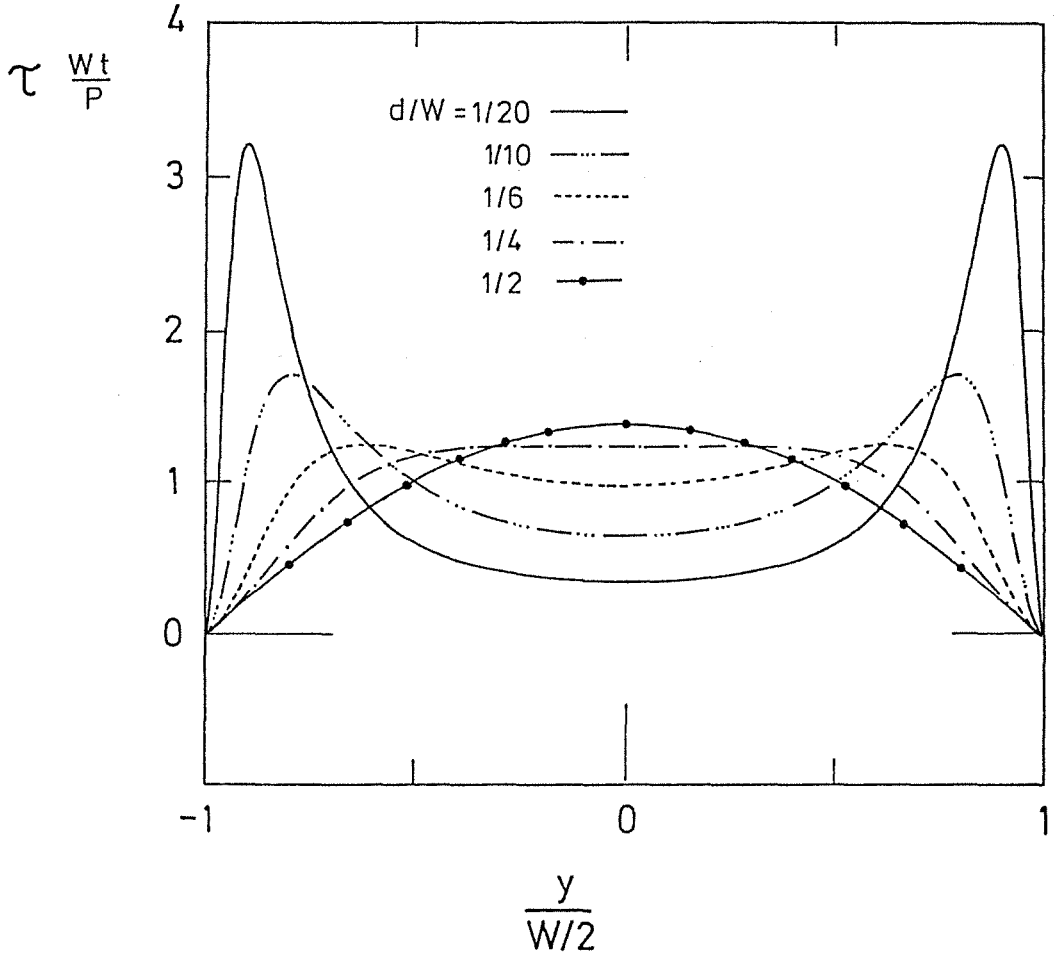

Fig.13

Shear stresses in the asymmetrically loaded bending bar at $x=0$.

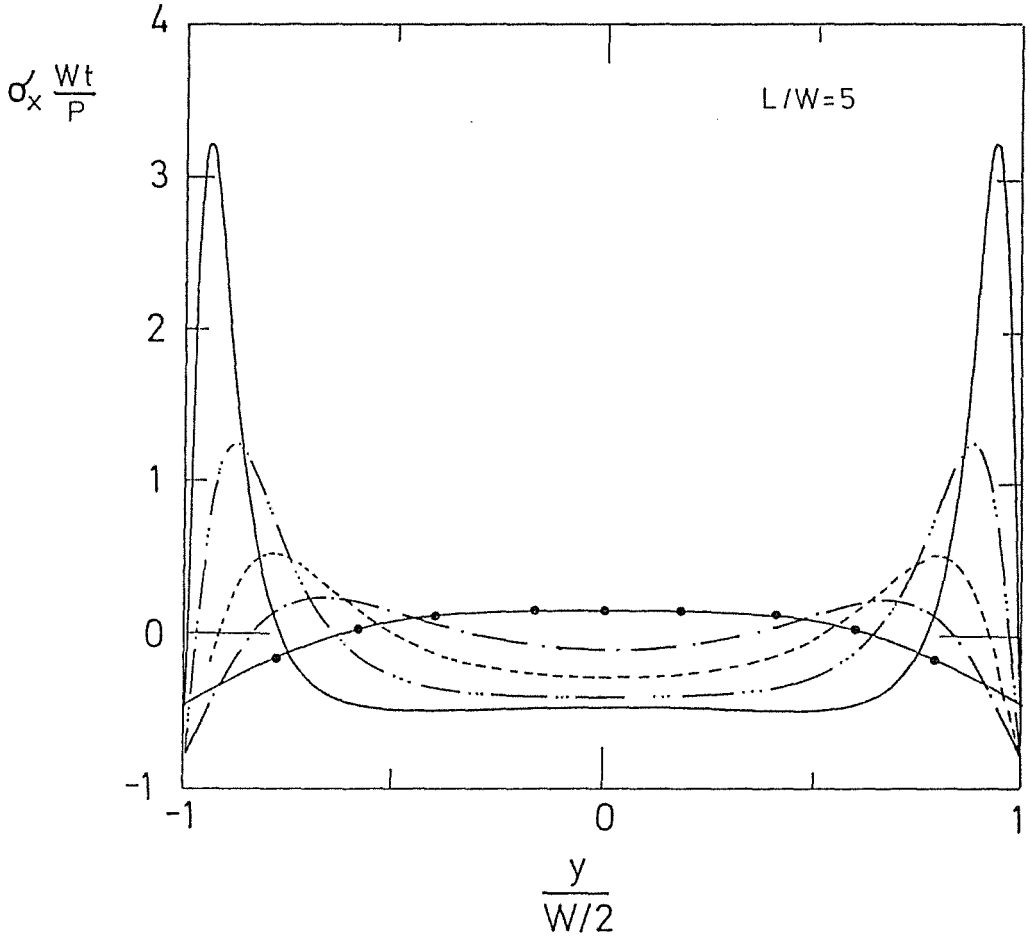

Fig.14

Normal stresses σ_x in the asymmetrically loaded bending bar at x=0 .

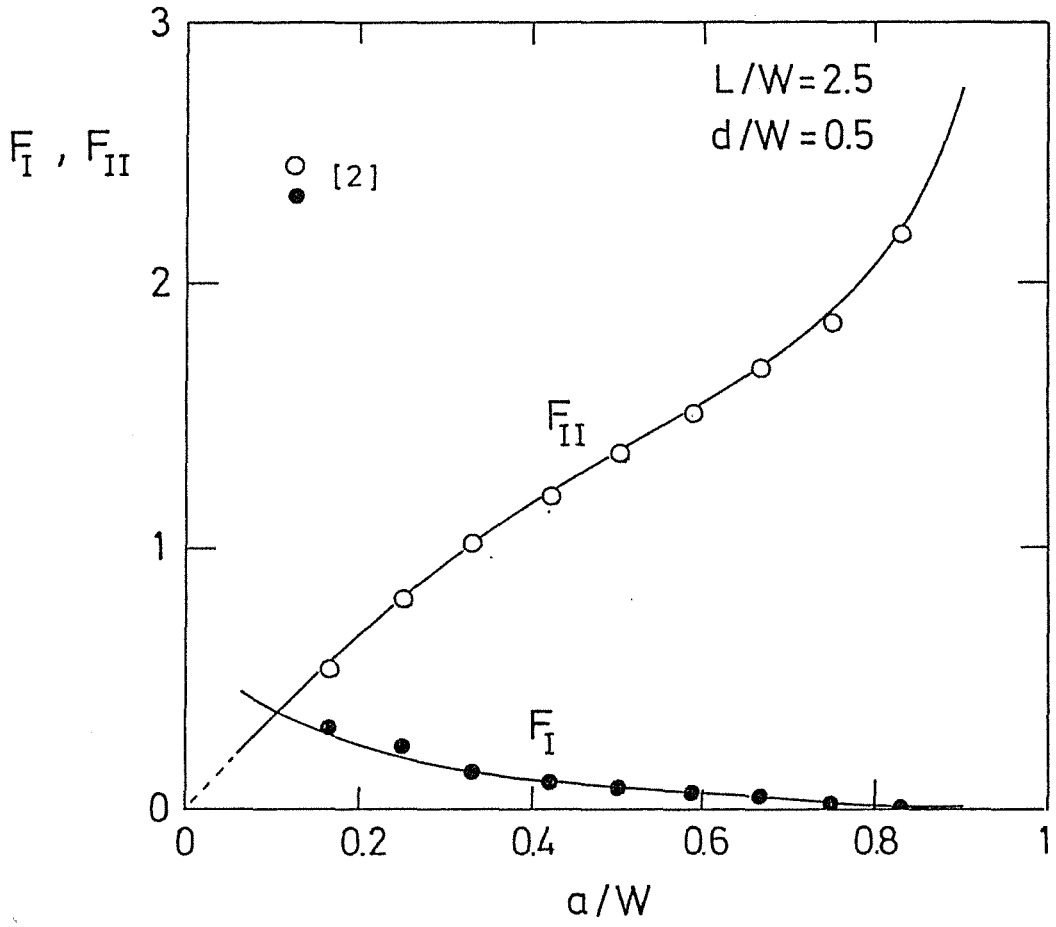

Fig.15

Geometric functions F_I and F_{II} compared with an FE-result from [12].

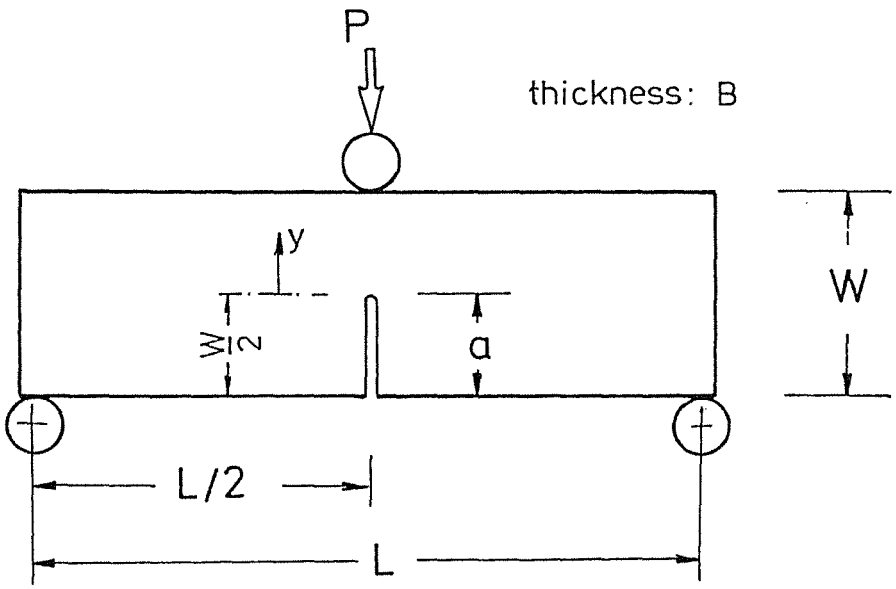

Fig.16

Edge-notched bending bar in a 3-point-bending test.

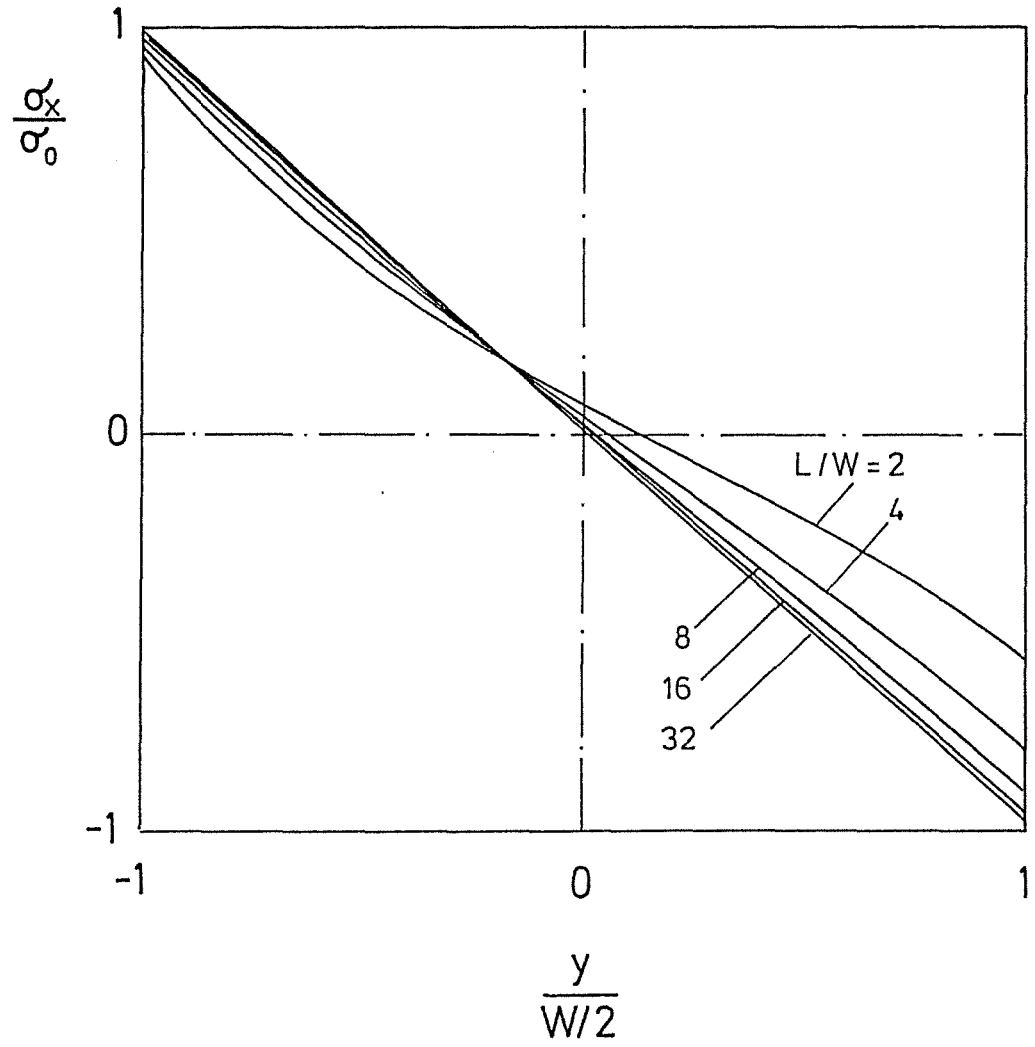

Fig.17

Stress distribution $\sigma_x(y)$.

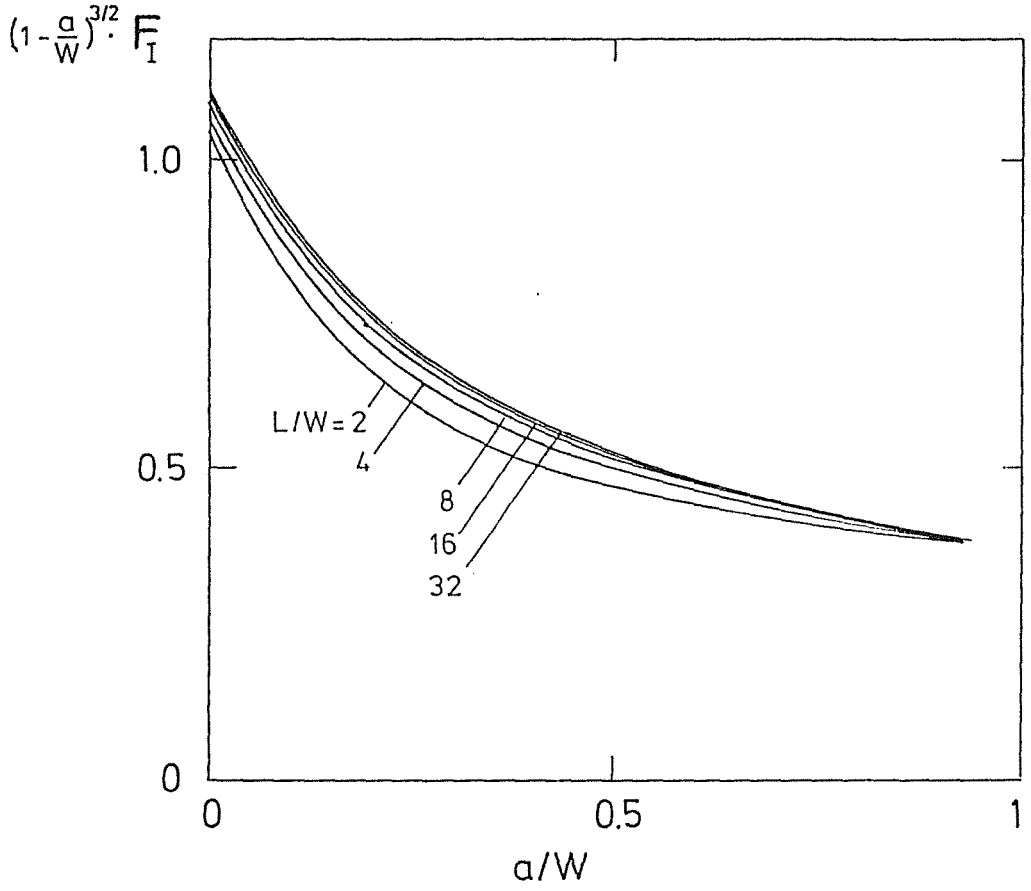

Fig.18

Geometric function in normalized form.

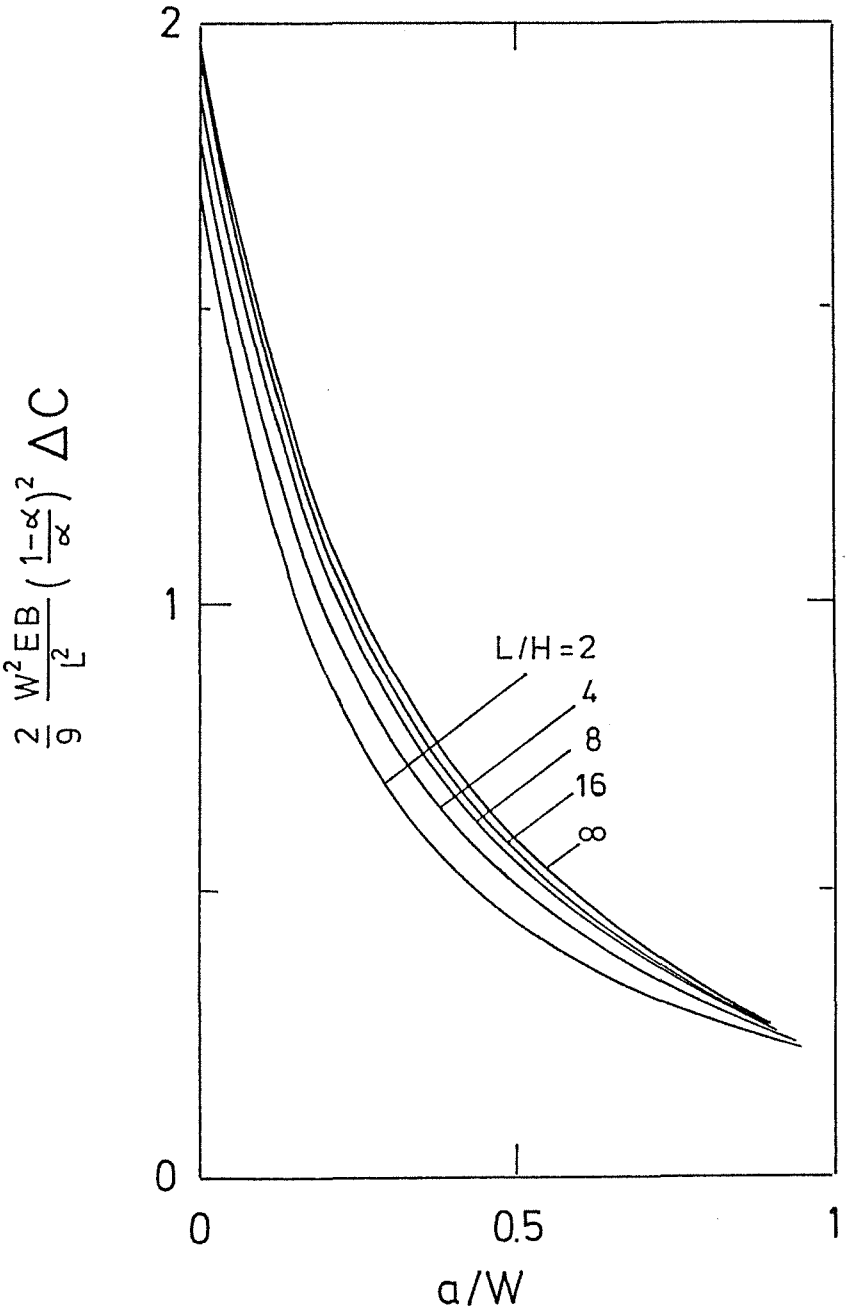

Fig.19

Compliance ΔC in normalized form.

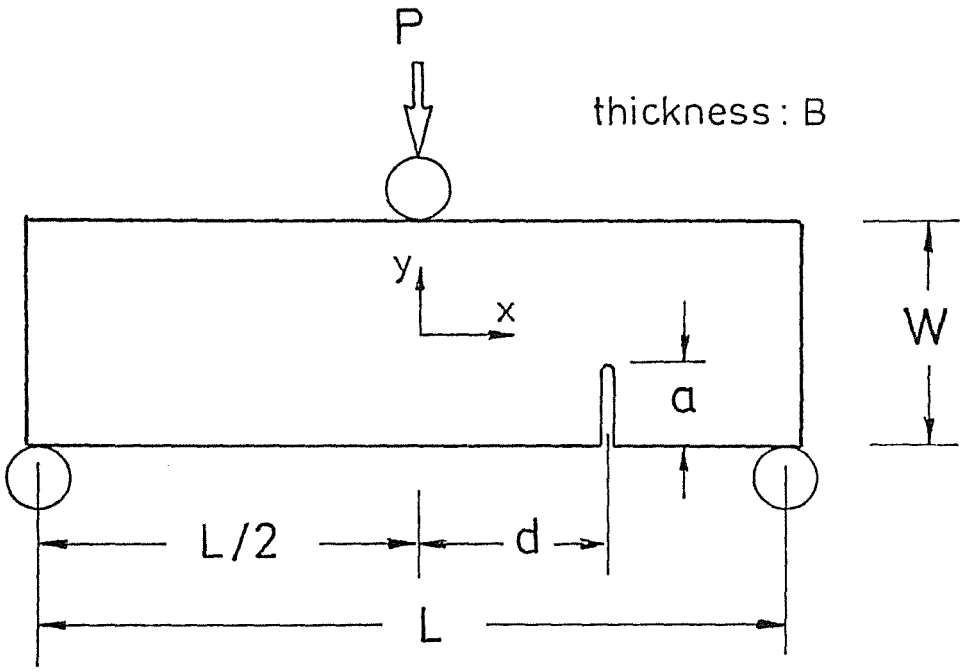

Fig.20

Bending bar with an eccentric edge-crack in a 3-point-bending test.

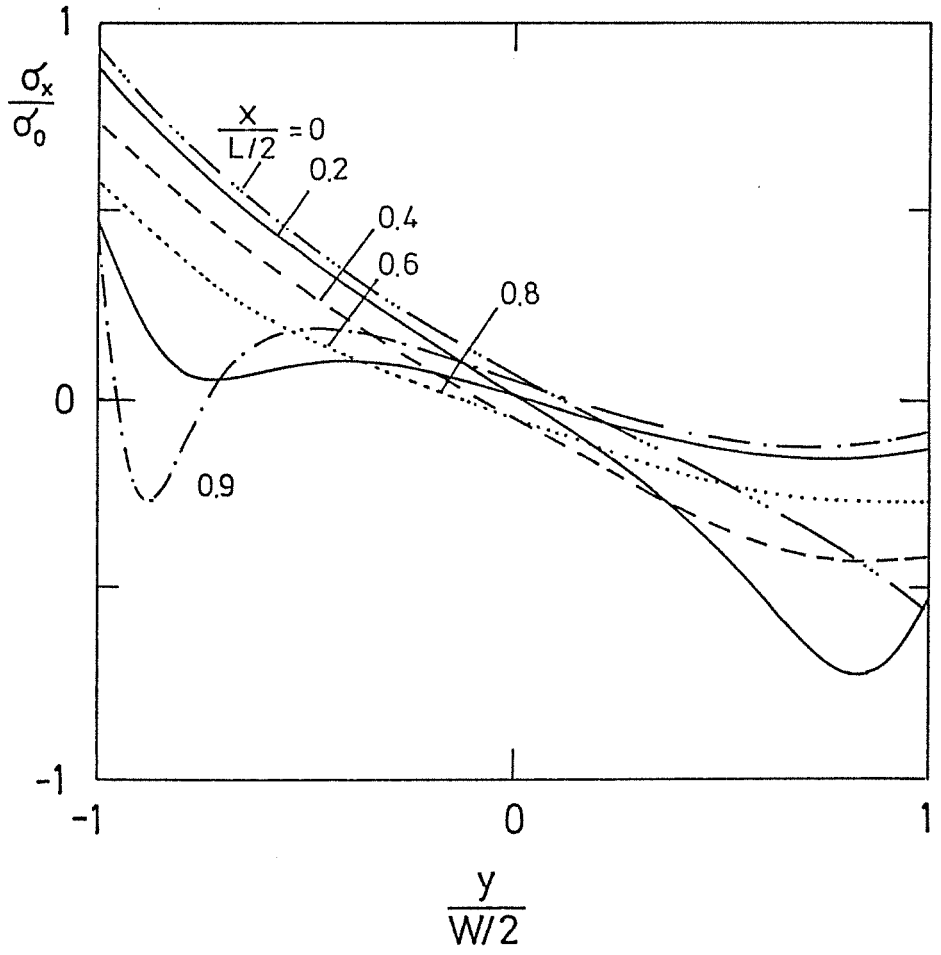

Fig.21

Stress distribution $\sigma_x(y)$.

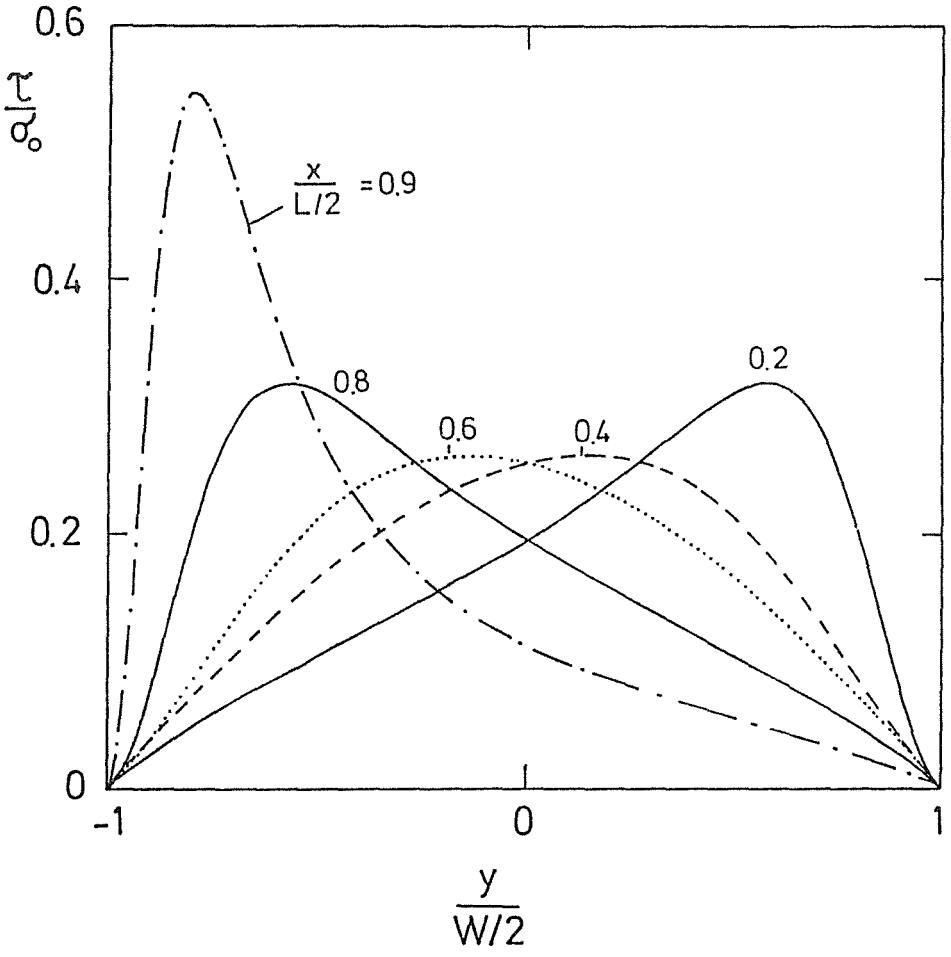

Fig.22

Stress distribution $\tau(y)$.

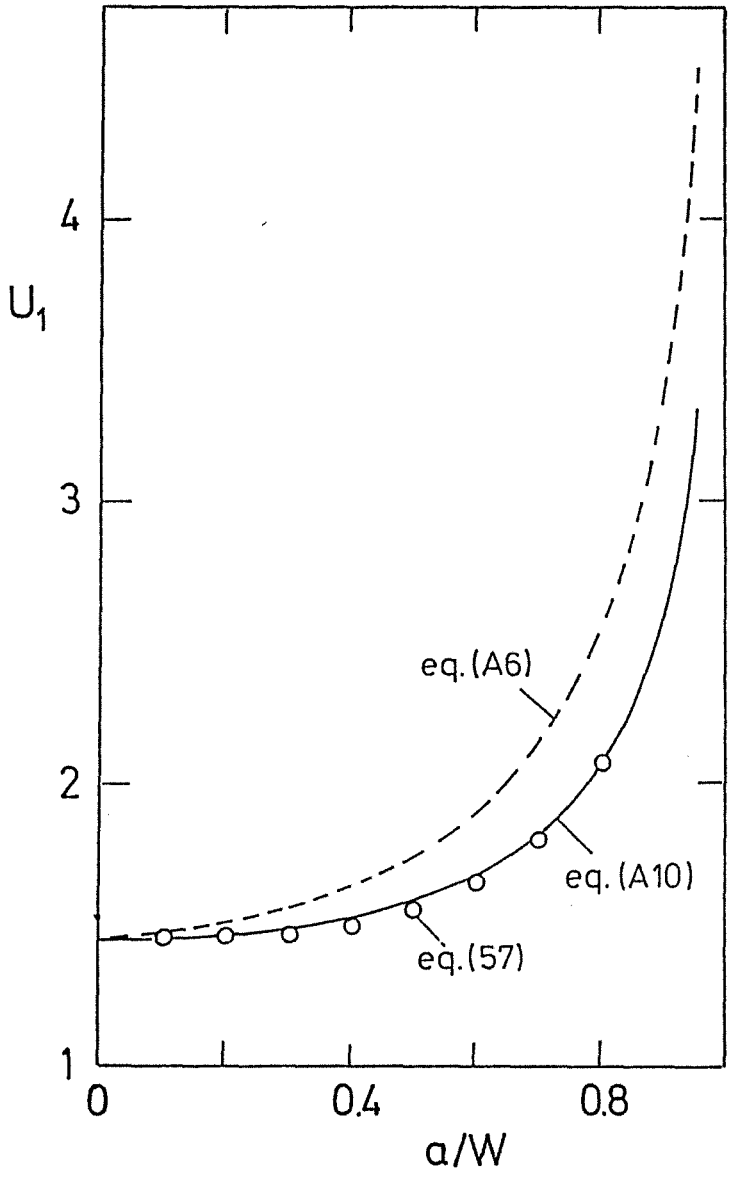

Fig.A1

Crack mouth opening compared with data from the literature.